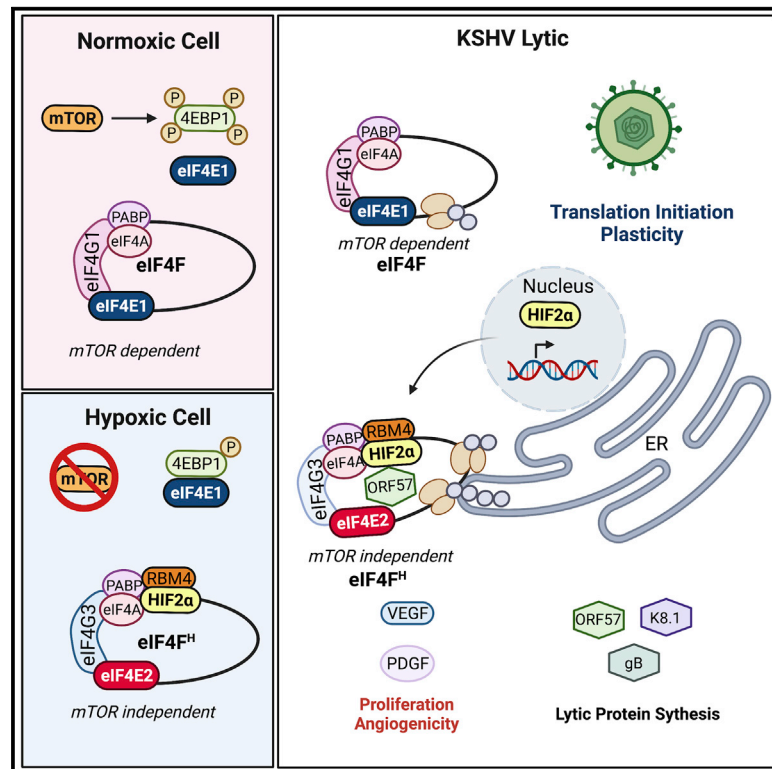


# Kaposi's sarcoma herpesvirus activates the hypoxia response to usurp HIF2 $\alpha$ -dependent translation initiation for replication and oncogenesis

## Graphical abstract



## Authors

Omayra Méndez-Solís,  
Mourad Bendjennat, Julian Naipauer, ...,  
Ethel Cesarman, Stephen Lee,  
Enrique A. Mesri

## Correspondence

stephenlee@med.miami.edu (S.L.),  
emesri@med.miami.edu (E.A.M.)

## In brief

Méndez-Solís et al. show that KSHV during the lytic phase upregulates and re-localizes HIF2 $\alpha$  to the ER to gain access to the alternative translation machinery eIF4F<sup>H</sup>. This KSHV “translation initiation plasticity” allows infected cells to translate viral and host proteins via mTOR-dependent or -independent mechanisms contributing to KSHV-induced sarcomagenesis.

## Highlights

- KSHV upregulates and localizes HIF2 $\alpha$  to the ER in normoxia for a translational role
- KSHV mRNAs are bound and translated by the eIF4E2/HIF2 $\alpha$ -containing complex eIF4F<sup>H</sup>
- eIF4F<sup>H</sup> contributes to translation of KSHV-induced sarcomagenic proteins
- KSHV-infected cells translate proteins via mTOR-dependent or -independent mechanisms



## Article

# Kaposi's sarcoma herpesvirus activates the hypoxia response to usurp HIF2 $\alpha$ -dependent translation initiation for replication and oncogenesis

Omayra Méndez-Solís,<sup>1,2</sup> Mourad Bendjennat,<sup>1,2,4</sup> Julian Naipauer,<sup>1,2</sup> Phaedra R. Theodoridis,<sup>1,3</sup> J.J. David Ho,<sup>1,3</sup> Ramiro E. Verdun,<sup>5,6</sup> Joshua M. Hare,<sup>6,7</sup> Ethel Cesarman,<sup>8</sup> Stephen Lee,<sup>1,3,\*</sup> and Enrique A. Mesri<sup>1,2,9,\*</sup>

<sup>1</sup>Tumor Biology Program, Sylvester Comprehensive Cancer Center, University of Miami Miller School of Medicine, Miami, FL 33136, USA  
<sup>2</sup>Miami Center for AIDS Research, Department of Microbiology and Immunology, University of Miami Miller School of Medicine, Miami, FL 33136, USA

<sup>3</sup>Department of Biochemistry and Molecular Biology, University of Miami Miller School of Medicine, Miami, FL 33136, USA

<sup>4</sup>Department of Radiation Oncology, University of Miami Miller School of Medicine, Miami, FL 33136, USA

<sup>5</sup>Cancer Epigenetics Program, Sylvester Comprehensive Cancer Center, University of Miami Miller School of Medicine, Miami, FL 33136, USA

<sup>6</sup>Department of Medicine, University of Miami Miller School of Medicine, Miami, FL 33136, USA

<sup>7</sup>Interdisciplinary Stem Cell Institute, University of Miami Miller School of Medicine, Miami, FL 33136, USA

<sup>8</sup>Department of Pathology and Laboratory Medicine, Weill Cornell Medicine, New York, NY 10021, USA

<sup>9</sup>Lead contact

\*Correspondence: [stephenlee@med.miami.edu](mailto:stephenlee@med.miami.edu) (S.L.), [emesri@med.miami.edu](mailto:emesri@med.miami.edu) (E.A.M.)

<https://doi.org/10.1016/j.celrep.2021.110144>

## SUMMARY

Kaposi's sarcoma herpesvirus (KSHV) is an angiogenesis-inducing oncovirus whose ability to usurp the oxygen-sensing machinery is central to its oncogenicity. By upregulating the hypoxia-inducible factors (HIFs), KSHV reprograms infected cells to a hypoxia-like state, triggering angiogenesis. Here we identify a link between KSHV replicative biology and oncogenicity by showing that KSHV's ability to regulate HIF2 $\alpha$  levels and localization to the endoplasmic reticulum (ER) in normoxia enables translation of viral lytic mRNAs through the HIF2 $\alpha$ -regulated eIF4E2 translation-initiation complex. This mechanism of translation in infected cells is critical for lytic protein synthesis and contributes to KSHV-induced PDGFRA activation and VEGF secretion. Thus, KSHV regulation of the oxygen-sensing machinery allows virally infected cells to initiate translation via the mTOR-dependent eIF4E1 or the HIF2 $\alpha$ -dependent, mTOR-independent, eIF4E2. This "translation initiation plasticity" (TRIP) is an oncoviral strategy used to optimize viral protein expression that links molecular strategies of viral replication to angiogenicity and oncogenesis.

## INTRODUCTION

Viral-based cancers are a consequence of molecular strategies for replication and persistence deployed by oncoviruses to control host-cell proliferation and survival (Mesri et al., 2014). Viruses control host translation to prioritize viral protein expression and to evade anti-viral responses during replication (Stern-Ginossar et al., 2019). Host anti-viral innate immune mechanisms include the reduction of protein synthesis through regulation of mRNA transcription and translation, processes that are often circumvented by viral immune evasion strategies such as skipping host protein synthesis shutoff and/or the use of internal ribosomal entry sites (IRESs) (Jackson, 2013; Walsh et al., 2013). Viruses generally target the initial step of translation involving the eIF4F initiation complex, which is composed of the cap-binding protein eIF4E1, scaffold protein eIF4G1, and helicase eIF4A1 (Walsh and Mohr, 2011). By regulating this translation complex formation, viruses influence global protein synthesis (Walsh and Mohr, 2011). Hypoxia is also known to inhibit eIF4F-mediated cap-dependent translation by promoting the association

between the cap-binding protein eIF4E1 and its repressor, 4EBP1, which cannot be phosphorylated by the lack of mTORC1 activation (Liu et al., 2006). Despite this inhibition of eIF4F formation, cells survive when oxygen is scarce through an alternative mTOR-independent eIF4F complex activated by HIF2 $\alpha$ , eIF4F<sup>H</sup>, which is composed of the cap-binding protein eIF4E2 (an eIF4E1 homolog not inhibited by 4EBP1), eIF4G3, eIF4A, and RBM4 (among other RNA-binding proteins) (Ho et al., 2016, 2020; Unacke et al., 2012). Mirroring eIF4F protein synthesis machinery in normoxia, eIF4F<sup>H</sup> supports efficient protein synthesis in hypoxia.

Kaposi's sarcoma associated herpesvirus (KSHV) is the etiologic agent of Kaposi's sarcoma (KS), an AIDS-associated cancer characterized by intense angiogenesis and proliferation of spindle-like cells (Mesri et al., 2010). The ability of KSHV to regulate protein translation and the hypoxia-inducible factors (HIFs) is central to KSHV-induced angiogenesis and its oncogenic potential (Cai et al., 2006; Carroll et al., 2006; Jham et al., 2011; Shin et al., 2008; Shrestha et al., 2017; Sodhi et al., 2000; Stern-Ginossar et al., 2019; Walsh and Mohr, 2011). KSHV angiogenic genes can modulate the AKT/mTOR axis, leading to activation



of the eIF4F complex through phosphorylation of the eIF4E1 inhibitor 4EBP1 to initiate translation of HIF1 $\alpha$ , which in turn drives the expression of VEGF (Arias et al., 2009; Cavallin et al., 2014; Jham et al., 2011; Tomlinson and Damania, 2004; Wang et al., 2006). This promotes proliferation and angiogenicity of the KSHV-infected cell (Jham et al., 2011; Sodhi et al., 2006). Additionally, HIF1 $\alpha$  and hypoxia are known to regulate gammaherpesviruses and KSHV replication and pathogenesis, which is consistent with the fact that KS tends to occur in the lower extremities of the body, where blood vessels are often poorly oxygenated (Davis et al., 2001; López-Rodríguez et al., 2019; Shrestha et al., 2017; Sternbach and Varon, 1995).

As KSHV infection upregulates the HIFs and metabolically reprograms infected cells, leading to a hypoxia-like environment in normoxia (Carroll et al., 2006; Viollet et al., 2017), we hypothesized that KSHV targeting of the oxygen-sensing machinery could be a vital part of KSHV replication strategy to enhance viral protein synthesis. Therefore, we investigated if KSHV, by regulating the HIFs, is enabled to use the hypoxic HIF2 $\alpha$ -regulated eIF4F<sup>H</sup> translation complex for initiation of viral protein synthesis in normoxia. Here, we show that the upregulation and ER localization of HIF2 $\alpha$  during lytic reactivation allows KSHV to use the alternative eIF4F<sup>H</sup> translation complex in normoxia for viral mRNA translation. This translation mechanism is necessary for viral replication and contributes to viral sarcomagenesis.

## RESULTS

### HIF2 $\alpha$ upregulation during KSHV lytic reactivation is necessary for efficient viral replication in normoxia

KSHV infection upregulates both HIF1 $\alpha$  and HIF2 $\alpha$  in normoxia (21% O<sub>2</sub>) (Cai et al., 2006, 2007; Carroll et al., 2006; Shin et al., 2008; Shrestha et al., 2017; Sodhi et al., 2000; Yogev et al., 2014). To study if KSHV affects HIFs levels upon lytic reactivation in normoxia, we used the doxycycline (DOX)-inducible KSHV producer cell line iSLK.KSHV219. This KSHV reactivation cell system contains a DOX-inducible KSHV lytic switch protein (RTA) construct in stably infected SLK cells with rKSHV219 that expresses GFP under the constitutive EF-1 promoter (infection marker) and RFP under the KSHV lytic PAN promoter (early lytic and reactivation marker) (Myoung and Ganem, 2011). DOX treatment of these cells induces RTA expression, resulting in KSHV reactivation and production of new infectious viral particles 48–72 h after induction (Figure 1A). After lytic phase induction in normoxia, we observed that HIF2 $\alpha$  protein levels underwent significant changes, unlike HIF1 $\alpha$  protein, which remained slightly affected (Figure 1B). Indeed, post-DOX treatment, HIF2 $\alpha$  protein levels fluctuated from upregulation (~3-fold increase) at 24 h to downregulation (~60% decrease), when cells started producing virions at 48–72 h (Figure 1B). In normoxia, HIFs are typically downregulated by proteasome-dependent degradation (Cockman et al., 2000). To test whether HIF2 $\alpha$  levels decrease at later time points of KSHV reactivation via the proteasome pathway, cells were treated with the inhibitor MG132. Proteasome inhibition prevented HIF2 $\alpha$  downregulation and increased HIF2 $\alpha$  protein levels (~10-fold 48 h post-DOX and ~12-fold 72 h post-DOX) (Figure 1B). We also found HIF2 $\alpha$  mRNA levels increased during lytic replication (Figure S1A).

These data indicate that modulation of HIF2 $\alpha$  throughout the lytic cycle is mediated by regulation of both HIF2 $\alpha$  protein and mRNA levels.

As HIF2 $\alpha$  is a key component of the hypoxia-inducible eIF4F<sup>H</sup> complex in addition to being a hypoxia-regulated transcription factor (Ho et al., 2016; Uniacke et al., 2012), we sought to investigate the potential role(s) of this oxygen-sensing machinery component in normoxic KSHV lytic replication. To this end, we silenced HIF2 $\alpha$  in iSLK.KSHV219 cells cultured in normoxia prior to DOX-induced lytic replication. To compare the impact of HIF2 $\alpha$  silencing on eIF4F<sup>H</sup> function with HIF1 $\alpha$ /2 $\alpha$  transcriptional activities, we silenced in parallel experiments HIF1 $\beta$ , the critical subunit of the transcriptionally active HIF1 and HIF2 heterodimers (Tian et al., 1997; Wang et al., 1995). We observed that HIF2 $\alpha$  silencing, but not HIF1 $\beta$  knockdown, resulted in ~50% reduction in KSHV reactivation as assessed by RFP expression at 48 h post-DOX (Figure 1C). These observed differences in reactivation were not related to either higher silencing efficiency of siHIF2 $\alpha$  versus siHIF1 $\beta$  or small interfering RNA (siRNA) treatment-associated cell death (Figures S2A and S2B). To measure the number of infectious virions produced by HIF2 $\alpha$ - and HIF1 $\beta$ -depleted cells over time, AD293 cells were infected with cell-free supernatants from these reactivated cells, and the number of GFP-positive AD293 cells was quantified to calculate the 50% tissue culture infective dose (TCID<sub>50</sub>). Both HIF2 $\alpha$  and HIF1 $\beta$  silencing led to a steep decrease in extent and kinetics of infectious KSHV virion production (Figure 1D; reduction compared with siControl at 72 h: siHIF1 $\beta$ , 92% reduction; siHIF2 $\alpha$ , 98% reduction). Analysis of viral protein expression showed that the reduction in virus production upon HIF2 $\alpha$  knockdown was concomitant with a robust decrease in KSHV lytic protein levels; shown are immediate-early (IE) lytic RTA and ORF45, early lytic ORF57, and late lytic K8.1 and gB (Figure 1E). Importantly, as shown in Figure S3, knockdown of HIF2 $\alpha$  does not reduce DOX-inducible RTA mRNA and protein levels. Thus, the bulk of the RTA we detect in Figure 1E comes from the virus and not from the exogenous RTA induced by DOX (Figure S3). On the other hand, suppression of HIF's transcriptional activity by HIF1 $\beta$  silencing reduced to a much lower extent RTA, gB, K8.1, and ORF45 protein levels and did not decrease ORF57 (Figure 1F). These reductions in HIF1 $\beta$ -silenced cells may be due to HIFs transcriptional involvement in KSHV replication, as previously shown (Shrestha et al., 2017).

We then assessed the effect HIF2 $\alpha$  and HIF1 $\beta$  silencing had on lytic mRNA and protein levels. We found that HIF2 $\alpha$  silencing was much more potent in reducing viral mRNA and protein levels (Figure 1G) than the silencing of HIF's transcriptional activity via HIF1 $\beta$  silencing (Figure 1H). As with the exception of the HIF2 $\alpha$ -responsive RTA, many of these genes do not have hypoxia-responsive elements (HREs) in their promoters, we reasoned that the profound impact of HIF2 $\alpha$  silencing in KSHV replicative cascade was due to a combination of transcriptional and post-transcriptional effects (Haque et al., 2003, 2006; Zhang et al., 2014). To evaluate if post-transcriptional mechanisms are involved in HIF2 $\alpha$  regulation of viral gene expression upon lytic replication, we determined the effect of HIF2 $\alpha$  silencing on viral mRNA and protein half-lives

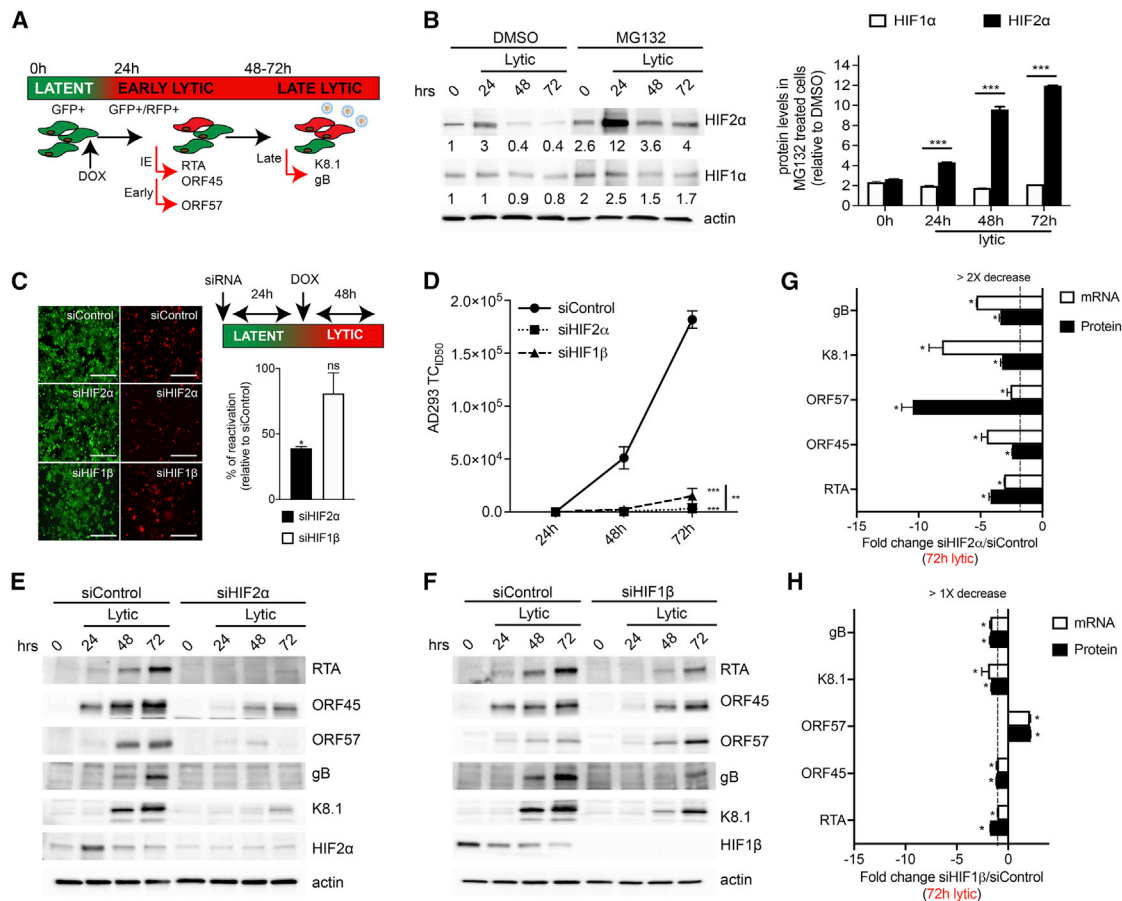


**Figure 1. HIF2 $\alpha$  upregulation during KSHV lytic reactivation is necessary for efficient viral replication in normoxia**

(A) Schematic diagram of iSLK.KSHV219 cell system. After doxycycline (DOX) treatment, these cells express the reactivation marker RFP driven by KSHV lytic PAN promoter and the immediate-early (IE) and early (E) protein levels increase. Forty-eight-hour to 72 h post-reattivation late lytic proteins are expressed and infectious virions are released.

(B) HIF1 $\alpha$  and HIF2 $\alpha$  protein levels before (0 h) and after (24–72 h) DOX treatment of iSLK.KSHV219 cells cultured in normoxia. MG132 prevents protein degradation via the proteasome. HIFs protein levels in DMSO and MG132 treated iSLK.KSHV219 cells (below corresponding immunoblot relative to 0 h DMSO; bar graph shows MG132 relative to DMSO) were calculated using ImageJ (n = 3; mean  $\pm$  SD; \*\*\*p < 0.0001, two-way ANOVA with Tukey's post-test).

(C) Pictures and percentage of reactivation 48 h post-DOX of siHIF2 $\alpha$  and siHIF1 $\beta$  iSLK.KSHV219 cells relative to siControl. siRNA transfection was performed 24 h prior to DOX-induced reactivation of KSHV. RFP expression driven by KSHV lytic PAN promoter was considered the reactivation marker and was measured using flow cytometry (n = 3; mean  $\pm$  SD; \*p < 0.001, unpaired t test). Scale bar, 100  $\mu$ m.

(D) Kinetics of infectious virion production of siControl, siHIF2 $\alpha$ , and siHIF1 $\beta$  iSLK.KSHV219 cells post-reattivation measured by AD293 TCID<sub>50</sub> (n = 3; mean  $\pm$  SD; \*p < 0.01, two-way ANOVA with Tukey's post-test).

(E) KSHV-encoded lytic protein levels in HIF2 $\alpha$ -silenced cells. Zero hours represents 24 h post-silencing and before DOX addition.

(F) KSHV IE, E, and late protein levels in siControl and siHIF1 $\beta$  iSLK.KSHV219 cells.

(G) Fold change of KSHV-encoded lytic mRNA and protein levels 72 h post-DOX in cells from (E) relative to siControl. Lytic mRNA levels were measured using qRT-PCR, and the lytic protein levels were determined using ImageJ (n = 3; mean  $\pm$  SD; \*p < 0.0001, two-way ANOVA with Tukey's post-test).

(H) Fold change of KSHV lytic genes mRNA and protein levels 72 h post-DOX in cells from (F) relative to siControl. KSHV lytic mRNA and protein levels were measured as in (G) (n = 3; mean  $\pm$  SD; \*p < 0.05, two-way ANOVA with Tukey's post-test).

by halting transcription and translation with actinomycin D (ActD) and cycloheximide (CHX), respectively, at 48 h post-lytic reactivation (Figure S4). Inhibition of transcription by ActD in HIF2 $\alpha$ -silenced cells did not further reduce the half-lives of viral transcripts compared with siControl (Figure S4B), while stopping translation using CHX did not affect significantly viral proteins turnover, as it was similar to siControl (Figure S4D). These results show that HIF2 $\alpha$  depletion does not increase the rate of either viral transcript or viral protein decay upon ActD and CHX

treatment (Figure S4). However, significant declines in protein levels of the glycoproteins K8.1 and gB and not their mRNA levels after ActD treatment was observed in HIF2 $\alpha$ -silenced cells, which points to a possible post-transcriptional role of HIF2 $\alpha$  (Figure S4C). Taken together, these results show that HIF2 $\alpha$  is critical for the expression of KSHV glycoproteins through a mechanism that is independent of active mRNA transcription in cells, pointing to a post-transcriptional role for HIF2 $\alpha$  in KSHV replication in normoxia.



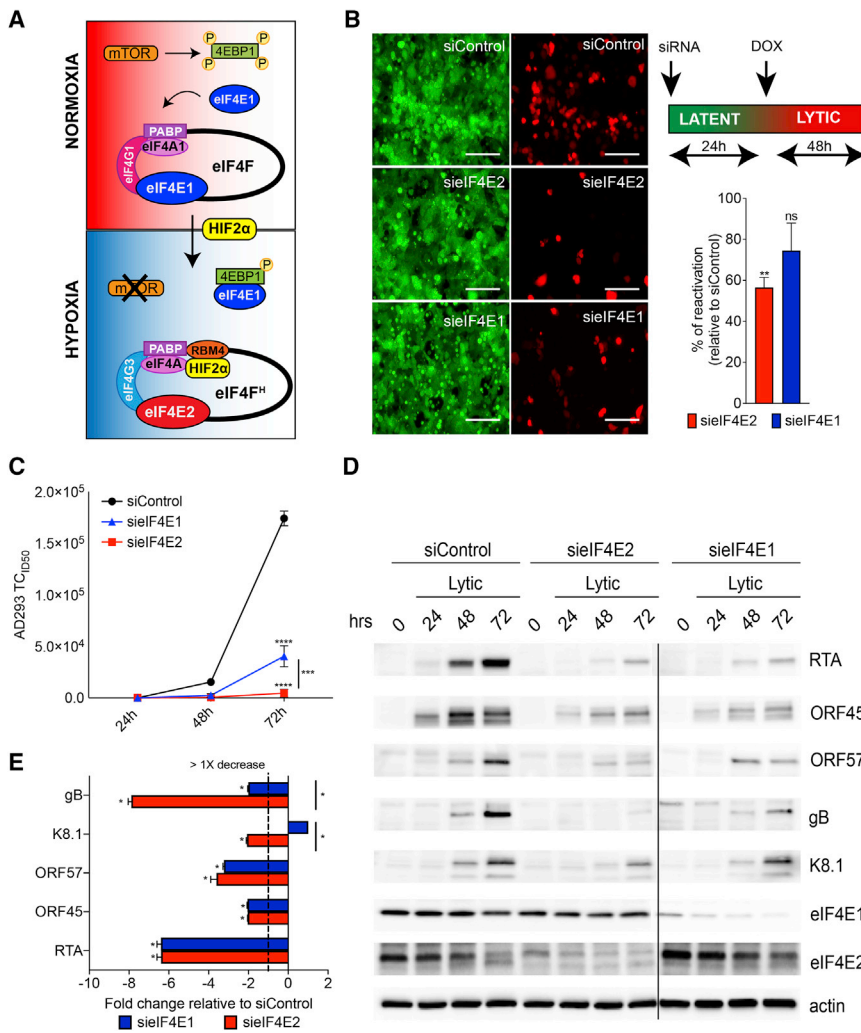


**Figure 2. eIF4E2 is essential for KSHV replication in normoxia**

(A) Oxygen-regulated switch in cap-dependent translation machinery. In normoxia, mTOR activity prevents sequestration of the cap-binding eIF4E1 protein by 4EBP1 for translation initiation. In hypoxia, HIF2 $\alpha$  stabilization and the absence of mTOR activity promotes the formation of the alternative eIF4F<sup>H</sup> protein synthesis machinery.

(B) Fluorescence microscope pictures and percentage of reactivation of sielF4E2 and sielF4E1 iSLK.KSHV219 cells relative to siControl 48 h post-DOX, measured using flow cytometry (n = 3; mean  $\pm$  SD; \*\*p < 0.01, unpaired t test). Cells were silenced as in Figure 1C. Scale bar, 100  $\mu$ m.

(C) Kinetics of infectious virion production after DOX treatment measured by AD293 TCID<sub>50</sub> (n = 3; mean  $\pm$  SD; \*\*\*p < 0.001 and \*\*\*\*p < 0.0001, two-way ANOVA with Sidak's post-test).

(D) KSHV-encoded protein levels in siControl, sielF4E2, and sielF4E1 iSLK.KSHV219 cells. Splicing of two different western blot images is indicated by the black line.

(E) Fold change of KSHV lytic protein levels in cells from (D) relative to siControl. Each bar represents the intensity of the corresponding western blot band 72 h post-DOX relative to siControl calculated using ImageJ (n = 3; mean  $\pm$  SD; \*p < 0.0001, two-way ANOVA with Tukey's post-test).

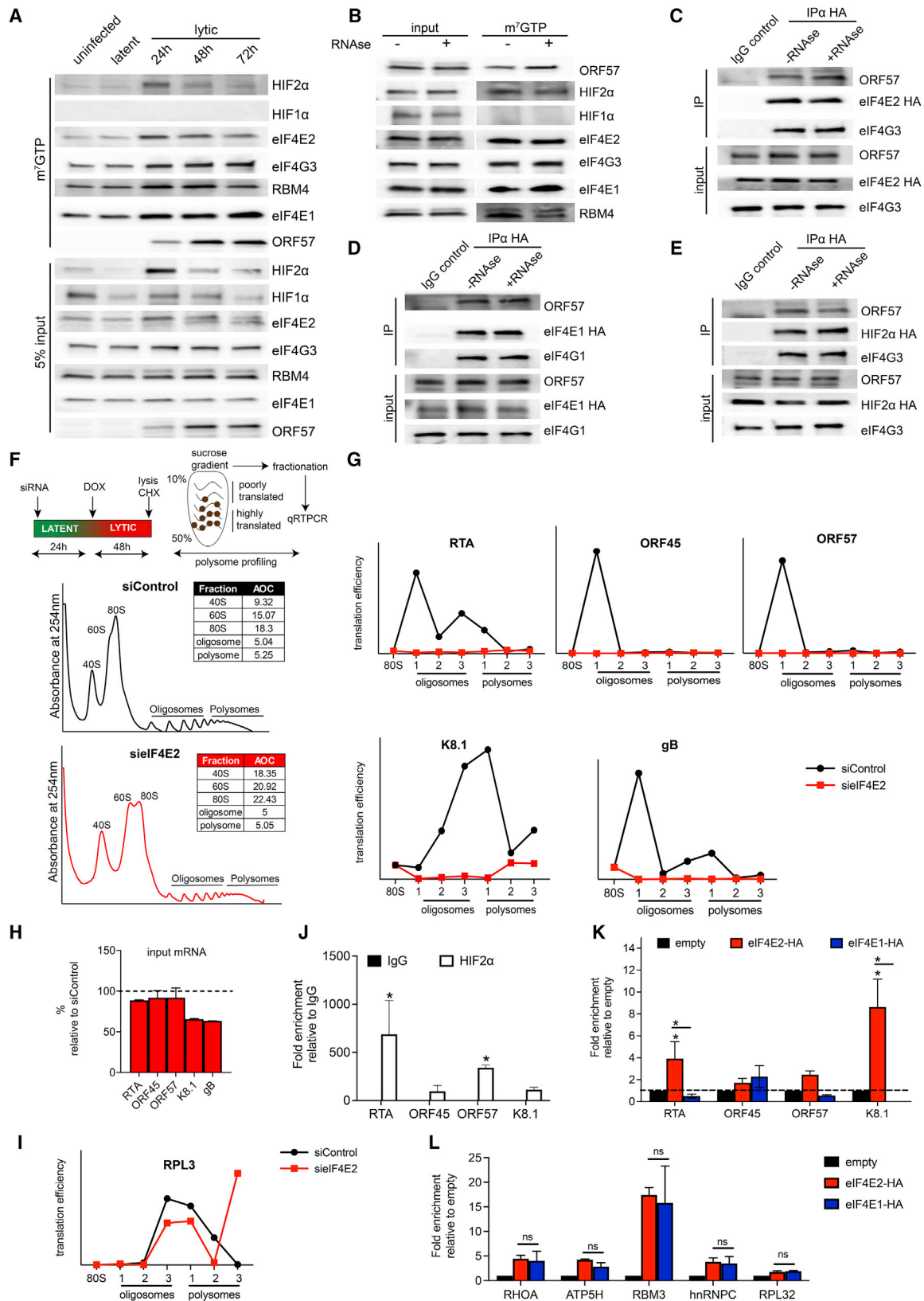
### eIF4E2 is essential for KSHV replication in normoxia

Our data suggest that HIF2 $\alpha$  could play a post-transcriptional role upon KSHV lytic reactivation in normoxia. Therefore, we evaluated the possibility that transient HIF2 $\alpha$  upregulation during KSHV lytic switch may allow hypoxia-like translation initiation via the HIF2 $\alpha$ -activated eIF4F<sup>H</sup> in normoxia (Figure 2A) by comparing the effects of eIF4E2 silencing, the cap-binding protein of eIF4F<sup>H</sup>, to eIF4E1 depletion, the cap-binding protein of the normoxic eIF4F complex. Similar to HIF2 $\alpha$  depletion, silencing of eIF4E2 prior to lytic reactivation, but not eIF4E1 knockdown, significantly reduced KSHV reactivation (Figure 2B). This suggests that the eIF4E2/HIF2 $\alpha$ -dependent translation initiation machinery is critical for the switch from latent state to reactivation of the virus. eIF4E2 silencing also resulted in greater than 95% decrease in infectious KSHV virion production (Figure 2C). Knockdown of the canonical eIF4E1 also reduced the production of infectious virions as previously reported (Pringle et al., 2019), albeit to a lower extent compared with sielF4E2 (85% reduction at 48 h and 77% reduction at 72 h compared with siControl) (Figure 2C).

Immunoblot quantification showed that the loss of eIF4E2 led to a much sharper decrease on the levels of KSHV glycoproteins gB and K8.1 compared with depletion of eIF4E1 (Figures 2D and 2E). Importantly, these observed differences were not due to sielF4E2 versus sielF4E1 silencing efficiency (Figure S2A). This indicates that upon KSHV lytic reactivation, eIF4E2-containing protein synthesis machinery is used to translate KSHV lytic mRNAs for viral replication. Together, these results suggest that KSHV manipulation of the oxygen-sensing machinery leading to HIF2 $\alpha$  upregulation enables the virus to use eIF4E2-mediated protein synthesis initiation in normoxia for optimal lytic protein synthesis, favoring viral replication.

### eIF4E2 initiates KSHV lytic protein synthesis in normoxia

As eIF4E2 and HIF2 $\alpha$  expression is required for lytic protein expression, we next investigated whether the eIF4E2/HIF2 $\alpha$ -containing cap-binding complexes were forming in normoxic lytically reactivated cells. To test this, we captured cap-binding complexes by m<sup>7</sup>GTP-conjugated agarose beads pull-downs. As displayed in Figure 3A, HIF2 $\alpha$  became a component of cap-binding protein complexes upon lytic reactivation. In addition, eIF4E2 and other components of the eIF4F<sup>H</sup> complex, RBM4 and eIF4G3, were also co-captured with HIF2 $\alpha$  in reactivated cells (Figure 3A). The canonical cap-binding protein eIF4E1 was present during latency and increased during reactivation.



(legend on next page)

In contrast, eIF4E2 was negligible before reactivation but robustly captured in the complexes after lytic induction (Figure 3A). These data indicate that eIF4E2 cap-binding complexes form upon KSHV lytic replication in normoxia.

KSHV-encoded ORF57 potently regulate viral mRNA translation, as was shown to be associated with the normoxic eIF4F complex through PYM (Boyne et al., 2010). We also found that ORF57 is part of cap-binding complexes during lytic replication and that its association is RNase resistant (Figures 3A and 3B). Interestingly, ORF57 co-immunoprecipitated in the presence or absence of RNase with eIF4E2 and HIF2 $\alpha$  in lytically reactivated cells, as it did with eIF4E1 (Figures 3C–3E). These results suggest that ORF57 association to the alternative eIF4F<sup>H</sup> complex could play a role in viral mRNA translation, with ORF57 being potentially a viral component involved in the formation and/or activity of this HIF2 $\alpha$ -activated complex.

As eIF4E2 translation-initiation complexes exist in reactivated cells in normoxia, we next examined the role of eIF4E2-mediated translation initiation on the efficiency of lytic viral mRNA translation. To this end, we performed polysome profiling experiments in eIF4E2-silenced iSLK.KSHV219 cells that were lytically induced (Figure 3F). eIF4E2 knockdown had no impact on either monosome or polysome formation and therefore no major effect on global mRNA translational status (Figure 3F). However, eIF4E2 knockdown dramatically reduced the translation efficiency of KSHV lytic mRNAs as measured using differential qRT-PCR of polysome profiling fractions (Figure 3G). The input mRNA level of the measured lytic genes was similar to siControl, demonstrating that decreased translation efficiency upon eIF4E2 knockdown was due to reduced association of these lytic viral mRNAs to ribosomes (Figure 3H). As control for a specific effect of eIF4E2 silencing, we also measured the translation efficiency of an eIF4E1-dependent host gene, RPL3, which was not affected by siIF4E2 silencing (Figure 3I) (Lenarcic et al., 2014). These results further support that eIF4E2 cap binding mediates initiation of KSHV lytic protein synthesis upon reactivation in normoxia.

To determine if lytic viral mRNAs were preferentially translated via HIF2 $\alpha$ /eIF4E2-containing initiation complexes in normoxia, we performed HIF2 $\alpha$ -, eIF4E2-, and eIF4E1-targeted RNA immu-

noprecipitation (RIP) using reactivated iSLK.KSHV219 cells. In the case of eIF4E2 and eIF4E1 RIP, iSLK.KSHV219 cells were transiently transfected with eIF4E1-HA, eIF4E2-HA, or empty vector plasmids before reactivation. As shown in Figure 3J, KSHV mRNA levels were substantially enriched (RTA, 700-fold; K8.1, 100-fold; ORF57, 400-fold; ORF45, 95-fold) after anti-HIF2 $\alpha$  RIP compared with the IgG control RIP. Similarly, KSHV mRNAs were enriched after eIF4E2-HA RIP (RTA, 4-fold; K8.1, 9-fold; ORF57, 3-fold; ORF45, 2-fold), albeit to a lower extent compared with endogenous HIF2 $\alpha$  RIP (Figures 3J and 3K). Moreover, lytic mRNAs were found to be preferentially associated with the HIF2 $\alpha$ /eIF4E2 complex compared with the eIF4E1 complex (Figures 3J and 3K). To determine the specificity of this translation mechanism for viral protein synthesis, we also measured the pull-down levels of several host genes known to be translated in normoxic conditions by eIF4E1 (Figure 3L) (Ho et al., 2016). We found that most of the measured host genes were enriched to a similar extent after eIF4E2 and eIF4E1 pull-downs, indicating that this alternative translation mechanism is not restricted to viral genes but preferentially used for viral mRNA translation initiation (Figures 3J–3L). Taken together, these results suggest a direct association of eIF4E2/HIF2 $\alpha$ -containing translation-initiation complexes with viral mRNAs during lytic reactivation in normoxia.

### HIF2 $\alpha$ co-localizes with the ER in KSHV-reactivated cells in normoxia

Our data showed that HIF2 $\alpha$  plays a translational role, as it is a component of cap-binding complexes and can associate with lytic mRNAs in reactivated cells. To further confirm this translation role, we tested whether HIF2 $\alpha$  re-localizes from the nucleus to the cytoplasm upon lytic replication by performing HIF2 $\alpha$  immunofluorescence (IF) in latent and reactivated iSLK.KSHV219 cells. Using deconvolution, we found that HIF2 $\alpha$  is localized predominantly in the nucleus (~95% [n = 200]) in latently infected (GFP-positive) iSLK.KSHV219 cells, while in reactivated cells (RFP-positive), HIF2 $\alpha$  is found mostly in perinuclear regions (~80% [n = 81]) (Figure 4A). In addition, HIF2 $\alpha$  shows a strong perinuclear localization in cells expressing ORF57 (~90% [n = 179]) (Figure 4B). In K8.1-expressing cells,

### Figure 3. eIF4E2 initiates KSHV lytic protein synthesis in normoxia

- (A) Cap-binding proteins pulled down with m<sup>7</sup>GTP agarose-beads from un-infected, latent, and reactivated iSLKs.  
 (B) m<sup>7</sup>GTP pulled-down viral and host proteins in the presence or absence of RNase, 24 h post-reactivation.  
 (C) eIF4E2-HA immunoprecipitation (IP) in 48 h reactivated iSLK.KSHV219.  
 (D) eIF4E1-HA-associated proteins 48 h post-reactivation.  
 (E) HIF2 $\alpha$ -HA IP 24 h post-reactivation.  
 (F) Polysome profiles of siControl and siIF4E2 iSLK.KSHV219 cells 48 h post-reactivation. Silenced cells 48 h post-DOX were treated with cycloheximide (CHX), and lysates were sedimented through sucrose gradients and fractionated, and viral mRNAs from each fraction were detected using qRT-PCR. Ribosome subunits (40S, 60S), monosomes (80S), oligosomes, and polysomes are indicated. The table shows the area under the curve (AOC) of each fraction.  
 (G) Translation efficiency of KSHV lytic mRNAs in cells from (F). KSHV mRNA levels in all fractions were measured using qRT-PCR (n = 3). Each fraction CT value was normalized to the 80S fraction CT.  
 (H) Input mRNA levels of KSHV lytic genes prior polysome profiling measured using qRT-PCR 48 h post-DOX relative to siControl (n = 3; mean  $\pm$  SD; \*p < 0.0001, two-way ANOVA with Sidak's post-test).  
 (I) Translation efficiency of eIF4E1-dependent host gene RPL3 in cells from (F). RPL3 mRNA levels in all fractions were measured as in (G).  
 (J) Fold enrichment of KSHV mRNAs after endogenous HIF2 $\alpha$  RNA immunoprecipitation (RIP) relative to IgG RIP control at 24 h post-DOX. KSHV mRNA levels were quantified using qRT-PCR, and CT values were first normalized to input CT (n = 3; mean  $\pm$  SD; \*p < 0.05, two-way ANOVA with Sidak's post-test).  
 (K) Pull-down levels of KSHV mRNAs after eIF4E2-HA and eIF4E1-HA RIP relative to empty control at 24 h post-DOX. KSHV mRNA levels were quantified as in (J) (n = 3; mean  $\pm$  SD; \*p < 0.05, two-way ANOVA with Tukey's post-test).  
 (L) Host gene pull-down levels in cells from (K) (n = 3; mean  $\pm$  SD; ns, not significant, two-way ANOVA with Tukey's post-test).

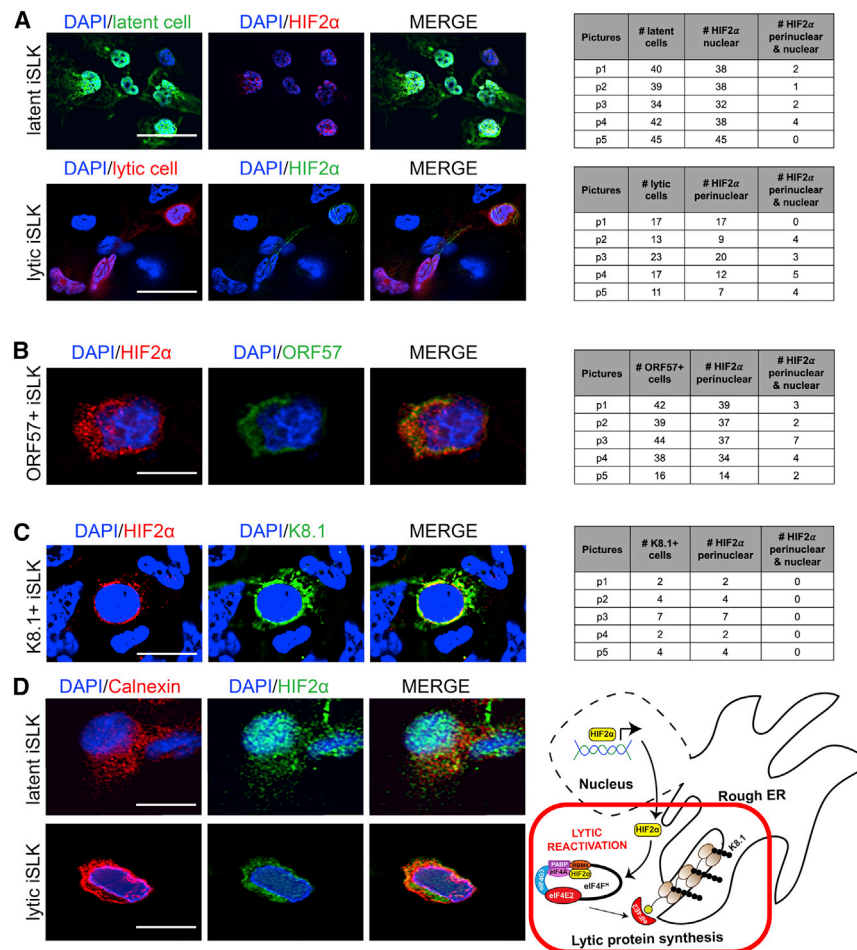


**Figure 4. HIF2 $\alpha$  co-localizes with the ER in KSHV-reactivated cells in normoxia**

(A) Representative three-dimensional (3D) fluorescence microscopy projections of HIF2 $\alpha$  staining in latent and lytic (DOX 72 h) iSLK.KSHV219 cells. The tables on the right show the quantification of HIF2 $\alpha$  nuclear and perinuclear localization in five representative pictures (40 $\times$  magnification). Scale bar represents 20  $\mu$ m.

(B) Representative HIF2 $\alpha$  immunofluorescence (IF) in ORF57-expressing iSLK.KSHV219 cells (DOX 72 h). The localization of HIF2 $\alpha$  was analyzed as in (A). Scale bar represents 10  $\mu$ m.

(C) IF of HIF2 $\alpha$  in K8.1-expressing iSLK.KSHV219 cells (DOX 72 h). As in (A), HIF2 $\alpha$  localization was analyzed. Scale bar represents 10  $\mu$ m.

(D) Representative HIF2 $\alpha$  IF in calnexin (ER marker) immunolabeled latent and lytic (DOX 72 h) iSLK.KSHV219 cells. Scale bar represents 10  $\mu$ m.

which represent cells in the late lytic stage, 100% of cells (n = 19) displayed perinuclear HIF2 $\alpha$  (Figure 4C). Furthermore, these two KSHV lytic proteins (ORF57 and K8.1), whose expression is among those most strongly affected by HIF2 $\alpha$  silencing (Figure 1E), were shown to co-localize with HIF2 $\alpha$ , further supporting the involvement of HIF2 $\alpha$  in lytic viral protein synthesis (Figures 4B and 4C).

As viral glycoprotein synthesis, such as K8.1, takes place at the rough endoplasmic reticulum (ER) located at the periphery of the nucleus, we next evaluated whether HIF2 $\alpha$  co-localizes with the ER in reactivated cells. As shown in Figure 4D, HIF2 $\alpha$  IF signal tends to overlap with calnexin (an ER-resident protein) signal in reactivated cells but not in latent cells. These data indicate that HIF2 $\alpha$  localization is regulated upon KSHV lytic switch to favor lytic proteins synthesis.

#### KSHV induces the hypoxia response to upregulate the HIF2 $\alpha$ /eIF4E2 translation-initiation complex in normoxia

Our results suggest that the ability of KSHV to induce a hypoxia-like state in infected cells by upregulating the HIFs allows the virus to use the HIF2 $\alpha$ /eIF4E2 translation initiation for efficient viral replication. In cancer cells, eIF4E proteins levels can be regulated by HIF1 $\alpha$  (Yi et al., 2013); therefore, we characterized the

possible mutual regulatory roles of the HIFs and eIF4E2-mediated translation by measuring the protein levels of HIF2 $\alpha$ , HIF1 $\alpha$ , HIF1 $\beta$ , and eIF4E2 in infected and un-infected cells silenced for the expression of HIF1 $\beta$ , HIF2 $\alpha$ , or eIF4E2. Depletion of HIF's transcriptional activity by HIF1 $\beta$  silencing resulted in decreased mRNA and protein levels of eIF4E2 and reduction in HIF2 $\alpha$  upregulation in infected cells (Figures 5A–5C). Moreover, the upregulation of HIF2 $\alpha$  that occurs in KSHV-infected cells 24 h post-lytic reactivation (Figure 1B) was fully suppressed by eIF4E2 silencing (Figures 5D and 5E).

Polysome analysis showed a significant decrease in the translation efficiency of HIF2 $\alpha$  after eIF4E2 knockdown (Figure 5F). Also, as observed for lytic mRNAs (Figures 3J and 3K), HIF2 $\alpha$  mRNA was found to be preferentially associated to eIF4E2, indicating that HIF2 $\alpha$  translation is initiated by the eIF4E2-containing cap-binding complex (Figure 5G). In contrast, HIF2 $\alpha$  knockdown did not decrease eIF4E2 protein levels in reactivated cells (Figure 5H). Taken together, our data suggest a feedforward mechanism for activation of eIF4E2-mediated translation initiation whereby KSHV-upregulated HIFs promote eIF4E2 expression. The eIF4E2-containing complex, in turn, fosters HIF2 $\alpha$  translation, further enhancing viral protein synthesis by activation of the eIF4F<sup>H</sup> complex, driving viral replication (Figure 5I).

#### KSHV activation of HIF2 $\alpha$ /eIF4E2 translation initiation favors productive infection and enhances lytic gene expression in hMSCs

To use a natural KSHV infection system relevant to sarcomagenesis, we used human mesenchymal stem cells (hMSCs) in which KSHV spontaneously undergoes lytic replication with virion production upon *de novo* infection (Lee et al., 2016; Naipauer et al., 2019). These cells were shown to be a natural human target for KSHV infection leading to viral oncogenesis (Lee et al., 2016; Li



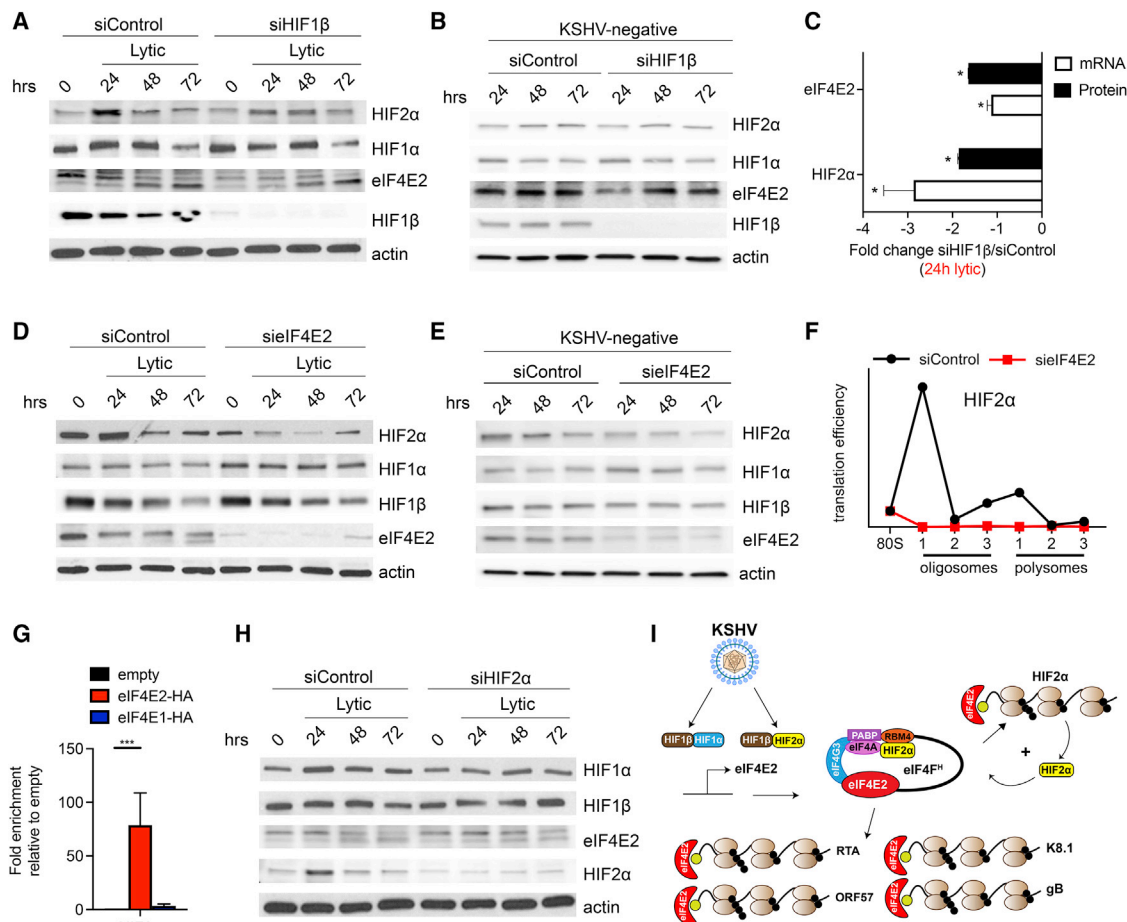


**Figure 5. KSHV induces the hypoxia response to upregulate the HIF2 $\alpha$ /eIF4E2 translation-initiation complex in normoxia**

(A) HIFs and eIF4E2 protein levels in normoxic siControl and siHIF1 $\beta$  iSLK.KSHV219 cells. These cells were silenced as in Figure 1.

(B) Expression of HIFs and eIF4E2 in siControl and siHIF1 $\beta$  KSHV-negative SLK cells.

(C) Fold change of eIF4E2 and HIF2 $\alpha$  mRNA and protein level relative to siControl at 24 h post-reactivation in cells from (A) (n = 3; mean  $\pm$  SD; \*p < 0.001, two-way ANOVA with Tukey's post-test).

(D) HIFs expression in siControl and siE4E2 iSLK.KSHV219 cells cultured in normoxia.

(E) HIFs protein levels in KSHV-negative SLK cells that were silenced with siControl or siE4E2.

(F) Translation efficiency of HIF2 $\alpha$  in siControl and siE4E2 iSLK.KSHV219 cells 48 h post-reactivation. HIF2 $\alpha$  mRNA levels in all fractions were measured using qRT-PCR (n = 3), and each fraction CT value was normalized to the 80S fraction CT.

(G) HIF2 $\alpha$  pull-down levels after eIF4E2 and eIF4E1 RIPs in reactivated cells 24 h post-DOX (n = 3; mean  $\pm$  SD; \*\*\*p < 0.0001, two-way ANOVA with Tukey's post-test).

(H) HIF1 $\alpha$ , HIF1 $\beta$ , and eIF4E2 protein levels in siControl and siHIF2 $\alpha$  iSLK.KSHV219 cells cultured in normoxia.

(I) Feedforward activation mechanism for eIF4E2 translation initiation in normoxia. KSHV-upregulated HIFs drive eIF4E2 expression, and the eIF4E2-containing complex allows HIF2 $\alpha$  translation, further enhancing viral mRNA translation initiation by eIF4E2.

et al., 2018). We have recently found that depending on the culture conditions at which human MSCs are maintained after KSHV infection, they can either behave as reservoirs for productive infection and KSHV dissemination (cultured in MSC media) or display PDGFRA-mediated proliferation characteristic of KSHV-driven sarcomagenesis (cultured in KS-like proangiogenic conditions) (Naipauer et al., 2019).

To evaluate in hMSCs the actual role of HIF2 $\alpha$ , we performed siRNA silencing of HIF2 $\alpha$  and HIF1 $\beta$  (for comparison of only transcriptional effects) prior to *de novo* rKSHV219 infection of normoxic hMSCs in MSC culture conditions that favor spontaneous lytic replication with virus production (Figure 6A) (Naipa-

uer et al., 2019). We found that HIF1 $\beta$  but not HIF2 $\alpha$  silencing significantly reduced the level of infection (~50% reduction relative to siControl) (Figure 6B). This indicates that HIF's joint transcriptional activities appear to be more important for *de novo* infection and latency establishment. On the other hand, HIF2 $\alpha$  silencing completely abolished KSHV lytic replication by robustly inhibiting KSHV reactivation (~97% reduction relative to siControl) and profoundly decreasing lytic mRNA and protein levels resulting in a clear-cut reduction of KSHV infectious virion production (Figures 6B–6E). These data show that HIF2 $\alpha$  is necessary for KSHV spontaneous lytic reactivation and replication in hMSCs.

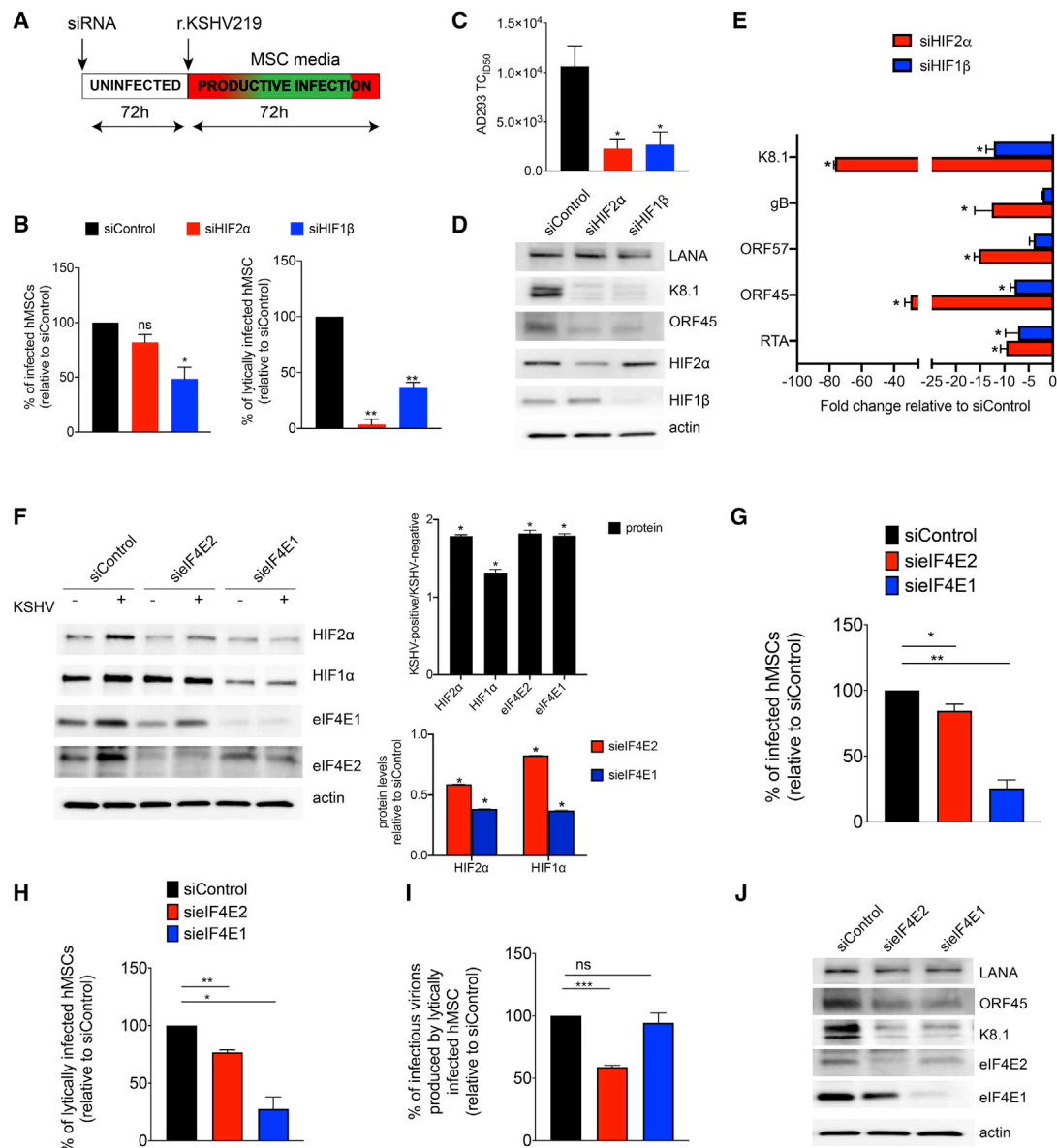


**Figure 6. KSHV activation of HIF2 $\alpha$ /eIF4E2 translation initiation favors productive infection and enhances lytic gene expression in hMSCs**

(A) Silencing approach used for primary *de novo* infected hMSCs cultured in normoxia. hMSCs were silenced for 72 h prior to infection with r.KSHV219 in MSC media.

(B) Percentage of siHIF2 $\alpha$  and siHIF1 $\beta$  infected hMSCs and percentage of lytically infected hMSCs 72 h post-infection (hpi) relative to siControl measured by flow cytometry (n = 3; mean  $\pm$  SD; \*p < 0.05 and \*\*p < 0.01, two-way ANOVA with Tukey's post-test).

(C) AD293 TCID<sub>50</sub> showing the number of infectious virions produced by siControl, siHIF2 $\alpha$ , and siHIF1 $\beta$  lytically infected hMSCs 72 hpi (n = 3; mean  $\pm$  SD; \*p < 0.01, two-way ANOVA with Tukey's post-test).

(D) KSHV-encoded proteins levels in hMSCs from (B).

(E) KSHV lytic mRNAs levels in cells from (B) relative to siControl measured by qRT-PCR (n = 3; mean  $\pm$  SD; \*p < 0.01, two-way ANOVA with Tukey's post-test).

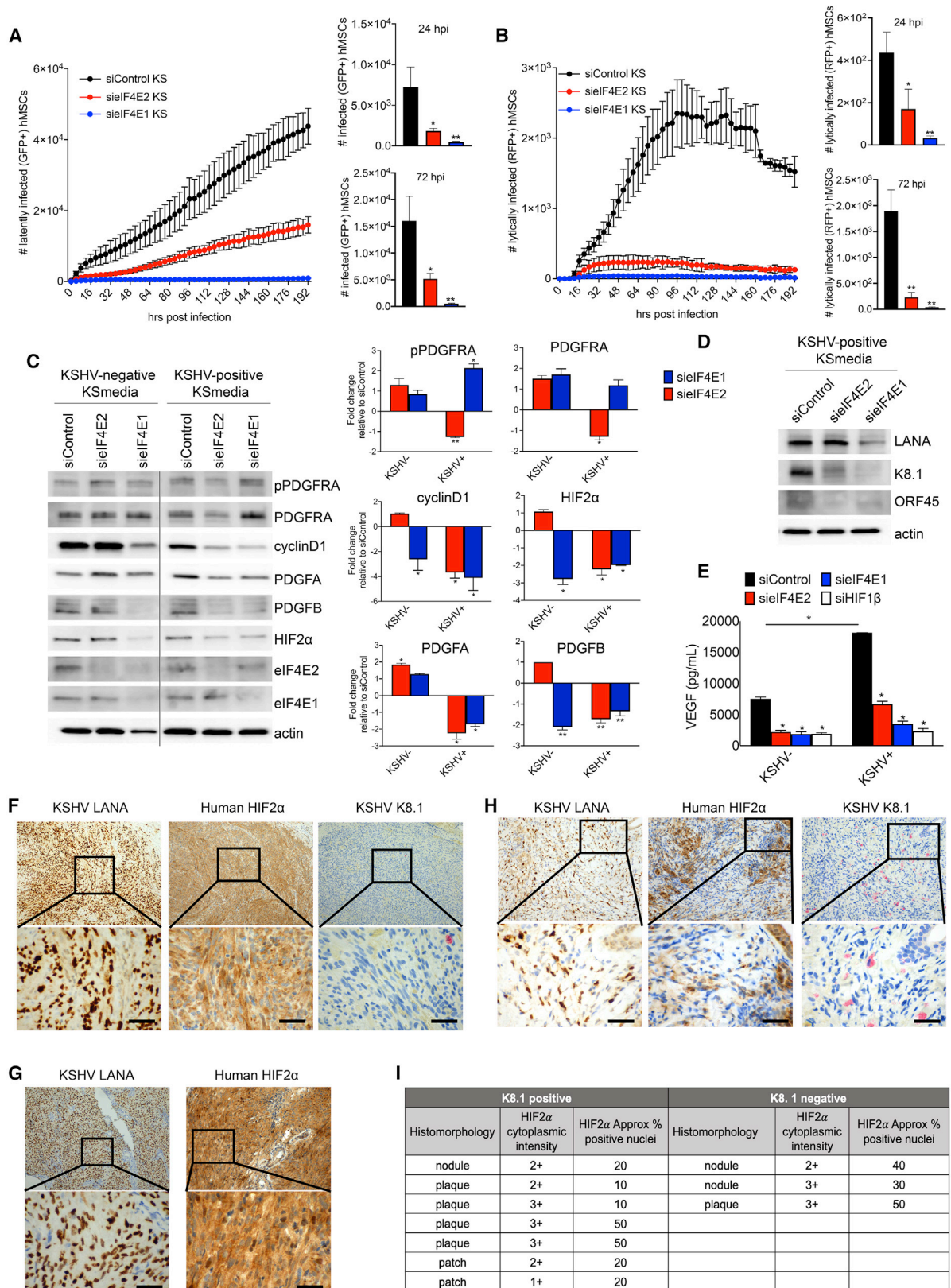
(F) HIFs protein level in normoxic siControl, sielF4E2, and sielF4E1 KSHV-positive (72 hpi) and KSHV-negative hMSCs. Protein levels were calculated using ImageJ (mean  $\pm$  SD; n = 3; \*p < 0.0001, two-way ANOVA with Tukey's or Sidak's post-test).

(G) Percentage of KSHV-infected hMSCs (GFP+ hMSC) 72 hpi relative to siControl. Infected GFP-expressing hMSC were measured by flow cytometry (mean  $\pm$  SD; n = 3; \*p < 0.05 and \*\*p < 0.01, unpaired t test).

(H) Percentage of lytically infected hMSCs (RFP-positive hMSCs) 72 hpi relative to siControl. RFP-expressing hMSCs were measured as GFP in (G) (mean  $\pm$  SD; n = 3; \*p < 0.05 and \*\*p < 0.01, unpaired t test).

(I) Percentage of infectious viral particles produced by sielF4E2 and sielF4E1 lytically infected hMSCs 72 hpi relative to siControl, measured by AD293 TCID<sub>50</sub> (mean  $\pm$  SD; \*\*\*p < 0.001; ns, not significant; unpaired t test).

(J) KSHV-encoded proteins levels in cells from (F).



(legend on next page)

We next compared the contribution of the HIF2 $\alpha$ -regulated eIF4E2 translation complex with its eIF4E1 counterpart, in KSHV-productive infection of hMSCs in normoxia. We found that KSHV infection of hMSCs induces HIF2 $\alpha$  and eIF4E2 protein upregulation 72 h post-infection (hpi) (HIF2 $\alpha$ ,  $\sim$ 2-fold; eIF4E2,  $\sim$ 2-fold) (Figure 6F). This shows that KSHV-mediated HIF2 $\alpha$  stabilization in normoxia does occur and could potentially lead to upregulation of the HIF2 $\alpha$ /eIF4E2-containing translation initiation machinery to support lytic replication (Figure 6F). We also found that HIF2 $\alpha$  protein level was reduced in eIF4E2-silenced KSHV-infected hMSCs relative to KSHV-positive siControl, while both HIF1 $\alpha$  and HIF2 $\alpha$  protein levels were decreased in eIF4E1-silenced hMSCs (Figure 6F). Notably, eIF4E2 depletion in hMSCs led to a 15% reduction in level of infection (number of GFP-positive hMSCs), whereas eIF4E1 silencing resulted in  $\sim$ 75% decrease compared with siControl 72 hpi (Figure 6G). As shown in Figure 6H, this reduction in *de novo* infection correlated with reduced numbers of lytically infected hMSCs (RFP-positive hMSCs) (relative to siControl at 72 hpi: siEIF4E2,  $\sim$ 20% reduction; siEIF4E1,  $\sim$ 70% reduction). Yet normalized to the level of infection, we found that siEIF4E2 lytically infected hMSCs produced  $\sim$ 40% less infectious virions, whereas siEIF4E1 hMSCs produced similar levels, both relative to siControl (Figure 6I). Immunoblot analysis showed reduced lytic protein levels, in particular IE lytic ORF45 and late lytic K8.1 (Figure 6J). This correlated with the decrease seen in infectious virions production from lytically infected hMSCs upon eIF4E2 silencing and with the decrease in level of *de novo* infection by eIF4E1 knockdown. These results suggest that establishment of *de novo* infection relies on eIF4E1-mediated translation initiation, while virion production in hMSCs as in the iSLK.KSHV219 reactivation system relies more heavily on eIF4E2 protein-synthesis initiation.

### The alternative eIF4E2 translation initiation contributes to KSHV-induced oncogenic mechanisms

KSHV activates host-mediated oncogenic mechanisms such as PDGFA/B activation of PDGFRA proliferative signaling and

VEGF-mediated angiogenicity that promotes the development of KS (Cavallin et al., 2018; Cesarman et al., 2019; Dittmer and Damania, 2016; Ganem, 2010; Mesri et al., 2010). This is mediated by KSHV oncogenes such as vGPCR that drive the production of host's PDGF ligands and VEGF via activation of the AKT-mTOR axis (Cavallin et al., 2014, 2018; Jham et al., 2011). We recently reported that although KSHV-infected hMSCs cultured in MSC media tend to develop a productive infection and stop proliferating shortly after KSHV infection (Naipauer et al., 2019), hMSCs cultured in KS-like conditions (endothelial and angiogenic growth factors rich media) are able to proliferate via ligand-mediated (PDGFA/B) activation of the PDGFRA signaling (Naipauer et al., 2019). Hence, we used them to gauge the contribution of eIF4E2- and eIF4E1-containing translation-initiation complexes to KS-related oncogenic and angiogenic mechanisms.

We silenced eIF4E2 or eIF4E1 prior to KSHV infection of hMSCs that were maintained in KS-like media after infection. Quantification of KSHV-infected (GFP-positive) and lytically infected hMSCs (RFP-positive) was performed using the IncuCyte Live-cell imaging and analysis system, as previously described (Naipauer et al., 2019). As shown in Figures 7A and 7B, eIF4E1 depletion severely decreased the establishment of KSHV infection in hMSCs (more than 90%) and fully blocked infected cell proliferation and lytic reactivation. eIF4E2 silencing led to a 75% reduction on establishment of infection at 24 h, reduced infected cell proliferation and impeded lytic reactivation in infected cells (Figures 7A and 7B). Importantly, this decrease seen in infection and infected cell proliferation is not a consequence of reduced proliferation of silenced hMSCs prior to infection (Figure S5). Western blot analysis at 72 hpi showed that the decrease in infection, proliferation, and reactivation by eIF4E1 and eIF4E2 silencing both occurred together with decreased levels of the PDGFRA ligands PDGF-A and PDGF-B and of the proliferation marker cyclin D1 (Figure 7C). Interestingly, eIF4E2 knockdown had more profound effects on PDGFRA protein level and activation in infected hMSCs cultured in KS-like media

### Figure 7. The alternative eIF4E2 translation initiation contributes to KSHV-induced oncogenic mechanisms

- (A) Number of infected hMSCs cultured in KS-like media. Infected human MSCs were incubated in an IncuCyte Zoom acquiring green fluorescence images. The number of infected cells was plotted over time, and bar graphs show 24 and 72 hpi (n = 3; mean  $\pm$  SD; \*p < 0.05 and \*\*p < 0.01, unpaired t test).
- (B) Number of lytically infected hMSCs cultured in KS-like media. The number of RFP expressing hMSCs was acquired as in (A) (n = 3; mean  $\pm$  SD; \*p < 0.05 and \*\*p < 0.01, unpaired t test).
- (C) Immunoblot of cyclinD1, HIF2 $\alpha$ , and PDGFRA wild-type (WT) and phosphorylated form and its cognate ligands (PDGFA and PDGFB) in silenced KSHV-negative and KSHV-positive hMSCs (72 hpi) cultured in KS media. Bar graph represents the fold change in the western blot band intensity of each protein relative to the siControl calculated using ImageJ (n = 3; mean  $\pm$  SD; \*p < 0.05, \*\*p < 0.001, and \*\*\*p < 0.0001, two-way ANOVA with Tukey's post-test).
- (D) KSHV proteins levels in silenced KSHV-positive hMSCs cultured in KS-like media 72 hpi.
- (E) VEGF secreted levels in cell-free supernatants of cells from (C). siHIF1 $\beta$  was used as a positive control for VEGF reduction (mean  $\pm$  SD; \*p < 0.0001, two-way ANOVA with Tukey's post-test).
- (F) Representative image of immunohistochemical (IHC) staining for HIF2 $\alpha$ , KSHV LANA, and K8.1 in a case of K8.1-positive nodular KS. Abundant cytoplasmic expression of HIF2 $\alpha$  (brown) was seen, as well as many cells with positive nuclei, in areas with numerous LANA<sup>+</sup> cells (brown). Only rare K8.1 positive cells (red) were seen. Magnification, 10 $\times$  (top) and 60 $\times$  (bottom). Scale bar, 50  $\mu$ m.
- (G) Representative HIF2 $\alpha$  and KSHV LANA IHC of a K8.1-negative case of nodular KS. Abundant cytoplasmic expression of HIF2 $\alpha$  was seen, as well as many cells with positive nuclei, in areas with numerous LANA<sup>+</sup> cells, but no K8.1 expression was seen. Magnification, 10 $\times$  (top) and 60 $\times$  (bottom). Scale bar, 50  $\mu$ m.
- (H) Representative image of IHC staining for HIF2 $\alpha$ , KSHV LANA, and K8.1 in a case of K8.1-positive plaque-stage KS. Cytoplasmic and nuclear expression of HIF2 $\alpha$  was seen in areas with numerous LANA<sup>+</sup> cells. K8.1-positive cells (red) were seen in these areas, indicative of lytic replication. Magnification, 10 $\times$  (top) and 60 $\times$  (bottom). Scale bar, 50  $\mu$ m.
- (I) Table showing ten selected cases for HIF2 $\alpha$  IHC, including seven cases with some K8.1-positive cells and three cases that were K8.1 negative, consistent with a tighter viral latency in these lesions. All cases had significant HIF2 $\alpha$  in the nuclei as well as cytoplasm of many cells independently of histopathological stage or evidence of lytic replication in the lesions.



(Figure 7C). These observed eIF4E2-dependent reductions correlated with reduced lytic protein levels and did not occur in siIF4E2 KSHV-negative hMSCs (Figures 7C and 7D). Thus, our results show that in infected hMSCs eIF4E2 silencing targets KSHV-induced host oncogenic mechanisms.

As VEGF is an important angiogenesis factor induced by KSHV genes and is found in KS lesions (Mesri et al., 2010), we measured the secreted levels of VEGF from infected cells. KSHV increased the secretion of VEGF from infected cells cultured in KS-like media (Figure 7E). Depletion of both eIF4E1 and eIF4E2 reduced the levels of secreted VEGF in KSHV-infected hMSCs, and this reduction correlated with decreased KSHV lytic protein levels (Figures 7D and 7E). Together our results show that both eIF4E1 and eIF4E2 translation initiation participate in KSHV oncogenesis, as KSHV-induced formation of the HIF2 $\alpha$ /eIF4E2 translation-initiation complex not only drives lytic viral protein synthesis but, together with eIF4E1, contributes to maintain PDGFA/B activation of PDGFRA proliferative signaling and VEGF angiogenicity.

Taken together, our *in vitro* and molecular data suggest that in the context of KS lesions, where lower oxygen levels may further increase HIFs levels, HIF2 $\alpha$  could play both transcriptional and translational roles in tumorigenesis and angiogenesis. To evaluate this *in vivo*, we stained clinical AIDS-KS lesions corresponding to different histological stages of KS for HIF2 $\alpha$  to determine whether its subcellular localization was consistent with a translational role during KSHV infection (Figures 1, 2, 3, 4, 5, and 6). Although the lesions showed KSHV-infected cells displaying nuclear HIF2 $\alpha$ , the occurrence of abundant cytoplasmic HIF2 $\alpha$  was found as a very common feature of all KS lesions we analyzed (Figures 7F–7I). This was observed regardless of whether these lesions displayed KSHV-infected spindle cells expressing the late lytic protein K8.1 (Figures 7F–7I). Thus, this suggests that HIF2 $\alpha$ 's dual role in the transcription and translation of viral and pathogenesis-related genes occurs broadly in KS lesions, pointing to a role of this branch of the oxygen-sensing machinery in oncogenicity and potential responses to therapies.

## DISCUSSION

The oncogenicity of KSHV stems from its capacity to usurp cellular mechanisms that drive infected cell survival and proliferation. Here we show that KSHV's ability to regulate the oxygen-sensing machinery allows the virus to translate proteins using the mTOR-dependent eIF4E1 or the alternative HIF2 $\alpha$ -activated eIF4E2-containing complex. This eIF4E2-dependent translation initiation is critical for expression of lytic proteins and for supporting activation of KSHV-induced oncogenic mechanisms. Thus, we propose "translation initiation plasticity" (TRIP) as a potential oncoviral adaptation to enhance mRNA translation during viral replication with oncogenic consequences.

Hypoxia and HIF1 $\alpha$  facilitate KSHV lytic replication, and KSHV upregulation of the HIFs is critical for its pathogenesis (Davis et al., 2001; Shrestha et al., 2017; Sodhi et al., 2000). Herein, we show that upon KSHV lytic switch, HIF2 $\alpha$  levels and subcellular localization are regulated to activate the alternative eIF4E2 translation initiation of viral mRNAs. It was recently shown that the KSHV lytic protein ORF34 is involved in HIF2 $\alpha$  stabilization

(Haque and Kousoulas, 2019). However, because in our system ORF34 has late early lytic expression, we suspect that other KSHV-related mechanisms are involved in the upregulation of HIF2 $\alpha$  occurring during lytic reactivation (Figure 1; Figure S1). We found KSHV early lytic gene ORF57 to interact with HIF2 $\alpha$  as early as 24 h post-reactivation and to co-localize with HIF2 $\alpha$  via immunofluorescence assessment, suggesting that ORF57 might be involved in the stabilization of HIF2 $\alpha$  in reactivated cells (Figures 3 and 4).

In our infection system, HIF2 $\alpha$  and eIF4E2 are necessary for efficient viral reactivation and replication. It has been proposed that in normoxia, eIF4E2 (also known as 4EHP) plays a repressive role by inhibiting eIF4E1 translation initiation (Chapat et al., 2017; Jafarnejad et al., 2018; Morita et al., 2012; von Stechow et al., 2015). Yet we found that in natural hypoxia or KSHV-induced hypoxia, HIF2 $\alpha$  upregulation enables translation initiation of eIF4E2-bound capped mRNAs. In seeking to further understand the connection of KSHV regulation of the HIFs with the activation of the eIF4F<sup>H</sup> complex in normoxia, we propose, on the basis of our data, that KSHV induction of HIF2 $\alpha$ -regulated translation is activated by a feedforward mechanism whereby HIFs promote the expression of eIF4E2. The eIF4E2 and ORF57-containing initiation complex enhances HIF2 $\alpha$  translation, thus increasing the availability of HIF2 $\alpha$ , boosting the formation of active eIF4F<sup>H</sup> complex in normoxia.

Viruses use diverse evasion strategies during replication to control eIF4E1 cap-dependent translation initiation (Walsh et al., 2013). This initial step of translation is regulated by mTORC1 that phosphorylates 4EBP1 releasing eIF4E1. When mTORC1 is inhibited, alternative translation machineries form in the cell (Figure 2A) (Ho and Lee, 2016). In the case of KSHV, mTOR activation is critical for its reactivation and KSHV encodes a plethora of mTOR activating early lytic genes (Jham et al., 2011; Pringle et al., 2019; Tomlinson and Damania, 2004; Wang et al., 2006). However, mTOR-mediated activation of eIF4E1 translation initiation was recently found to be dispensable for KSHV late lytic protein expression and for production of infectious virions (Pringle et al., 2019). In our study, we show that KSHV does use the alternative eIF4F<sup>H</sup> complex that is independent of mTORC1 activity for viral replication. As KSHV, an increasing number of viruses of global health importance, including severe acute respiratory syndrome coronavirus-2 (SARS-CoV-2), were shown to regulate the HIFs (Bojkova et al., 2020; Duette et al., 2018; Guo et al., 2014; Ren et al., 2019; Wakisaka et al., 2004), suggesting that full elucidation of this mechanism could lead to the development of pan-viral inhibitors targeting this host axis, which we now show could be critically necessary for viral replication. Moreover, these findings suggest that this virally prompted translation mechanism could give KSHV and possibly other viruses several adaptive advantages such as replication in different oxygen conditions and evasion of anti-viral responses that target the canonical eIF4F machinery.

Previous studies have shown and proposed a non-transcriptional role for HIF2 $\alpha$  in the cytoplasm (Park et al., 2003; Persson et al., 2020; Talks et al., 2000; Uniacke et al., 2012). During hypoxia, HIF2 $\alpha$  becomes a translation activating factor, and a neuroblastoma model shows that HIF2 $\alpha$  accumulates in the cytoplasm

promoting cell survival and tumor development independently from HIF1 $\beta$  (Persson et al., 2020; Uniacke et al., 2012). Our data showed that during KSHV lytic switch, HIF2 $\alpha$  becomes part of cap-binding complexes to participate in translation of lytic KSHV mRNAs, and in order to carry out this post-transcriptional function, it re-localizes to the periphery of the ER (Figures 3 and 4). HIF2 $\alpha$  re-localization to the ER during lytic replication and its co-localization with lytic viral proteins reinforce the evidence for HIF2 $\alpha$  role in KSHV lytic mRNA translation in normoxia.

We confirmed that eIF4E2 translation initiation is active and promotes lytic protein synthesis in productive and in KS-like hMSC infection models (Figures 6 and 7). Noticeably, HIF2 $\alpha$  silencing, in contrast to HIF1 $\beta$  inhibition, abolished KSHV lytic replication, illustrating how critical the dual roles of HIF2 $\alpha$  are in natural infection systems and pointing to HIF2 $\alpha$  as a very attractive anti-viral target. There is ample evidence that KSHV-encoded lytic proteins are needed for KSHV-mediated tumorigenesis (Cavallin et al., 2014, 2018; Dittmer and Damania, 2016; Ganem, 2010; Mesri et al., 2014). KSHV sarcomagenesis is thought to occur through a paracrine oncogenesis mechanism mediated by VEGF and PDGF that stimulates angiogenesis and proliferation of lytically and latently infected cells (Cavallin et al., 2014; Ganem, 2010; Mesri et al., 2010). We recently showed that PDGFRA is an oncogenic driver and therapeutic target in KS (Cavallin et al., 2018). More important, we found that KSHV lytic genes such as vGPCR are critical for the activation of the oncogenic signaling of PDGFRA through upregulation of its activating ligands PDGFB and PDGFA (Cavallin et al., 2018). Here, we show that PDGF expression leading to activation of PDGFRA and VEGF secretion in infected hMSCs cultured in KS-like conditions also relies on eIF4E2 (Figure 7). These observations suggest that eIF4E2 may complement the proposed AKT/mTOR/HIF1 $\alpha$ -mediated activation of VEGF and PDGF driven by KSHV oncogenes, strongly pointing to a possible role of “TRIP” in KSHV sarcomagenesis (Cavallin et al., 2018; Jham et al., 2011; Sodhi et al., 2006).

eIF4E2-driven translation is not only involved in protein synthesis in cells experiencing hypoxia but is also required for translation in the hypoxic core of tumors (Uniacke et al., 2014). We found by immunohistochemical detection that the activator of this translation complex (HIF2 $\alpha$ ) is strongly expressed in all stages of AIDS-KS, in accordance with prior reports (Carroll et al., 2006; Catrina et al., 2006). More important, in all the lesions HIF2 $\alpha$  localizes in both the nucleus and the cytoplasm, regardless of whether the lesions displayed or not lytically infected cells expressing K8.1 (Figures 7F–7I). Although this is in sharp contrast to our *in vitro* results, in which HIF2 $\alpha$  was upregulated as a consequence of KSHV regulation of the oxygen-sensing machinery during lytic replication, the robust level of cytoplasmic HIF2 $\alpha$  in KS is likely the consequence of viral effects and environmental oxygen levels that tend to stabilize the HIFs. HIF2 $\alpha$  subcellular localization is consistent with its dual role in transcription and in promoting eIF4E2 translation initiation in AIDS-KS tumors. Interestingly, HIF2 $\alpha$  overexpression and oncogenicity appear not to be a feature of non-viral sarcomas, where HIF2 $\alpha$  has been shown to have a tumor-suppressive role (Nakazawa et al., 2016). This underscores the importance of HIF2 $\alpha$  upregulation mechanism(s) driven by KSHV infection and its role in viral

replication and oncogenesis. The activation of eIF4E2 translation by cytoplasmic HIF2 $\alpha$  in KSHV-infected AIDS-KS tumors may potentially explain the host cells’ resistance to currently used therapies targeting the mTOR/eIF4E1 pathway such as Rapalogs (Krown et al., 2012; Stallone et al., 2005) or PDGFRA inhibitors (Cavallin et al., 2018; Koon et al., 2014).

Our findings suggest the possibility that the host and viral machinery underlying eIF4E2-driven translation might improve targeted therapies by uncovering targets for KS treatment and other virally induced cancers. We showed how KSHV regulation of the oxygen-sensing machinery changes the cell environment, to promote translation initiation plasticity for viral and host protein synthesis at different oxygen levels. This is a capability directly linked to the oncogenic outcome of KSHV infection in the host at the crossroads of oxygen levels, viral replication, and angiogenesis. It points to a remarkable oncoviral mechanism of host control and a plethora of anti-viral therapeutic targets.

### Limitations of the study

Our data show the involvement of HIF2 $\alpha$  in the translation of viral lytic genes and point to a role of eIF4F<sup>H</sup> in KSHV-induced sarcomagenesis. This needs to be confirmed in other available models of spontaneous lytic infection, such as the one recently described in lymphatic endothelial cells (LECs) (Golas et al., 2019), and through generation of knockout cells using CRISPR-Cas9. The actual contribution to sarcomagenesis could be evaluated *in vivo* by testing the tumorigenicity of knockout cells in our MSC-based KSHV infection to tumorigenesis model (Naipauer et al., 2019).

### STAR★METHODS

Detailed methods are provided in the online version of this paper and include the following:

- KEY RESOURCES TABLE
- RESOURCE AVAILABILITY
  - Lead contact
  - Materials availability
  - Data and code availability
- EXPERIMENTAL MODEL AND SUBJECT DETAILS
  - Cell lines
  - Primary cell cultures
  - Human tissue samples
- METHOD DETAILS
  - Transient RNA interference
  - Lytic Induction and AD293 TCID<sub>50</sub>
  - hMSCs *de novo* infection with rKSHV219
  - Western blotting (WB)
  - Flow cytometry
  - Real-time quantitative PCR (RT-qPCR)
  - Polysome profiling
  - RNA immunoprecipitation (RIP)
  - Cell proliferation assay (IncuCyte)
  - Enzyme-linked immunosorbent assay (ELISA)
  - M<sup>7</sup>GTP pulldowns
  - Protein immunoprecipitation (IP)
  - Immunofluorescence (IF)

- Immunohistochemistry of KS tumors
- **QUANTIFICATION AND STATISTICAL ANALYSIS**
- **ADDITIONAL RESOURCES**

#### SUPPLEMENTAL INFORMATION

Supplemental information can be found online at <https://doi.org/10.1016/j.celrep.2021.110144>.

#### ACKNOWLEDGEMENTS

We would like to thank Dr. Darlah López-Rodríguez and Dr. Santas Rosario for their technical support and Dr. Mariana Schlesinger and Zelmira Nuñez del Prado for manuscript editing and scientific insight. We want to thank the Flow Cytometry Core Facility for assistance with flow cytometry and cell sorting analysis. The IncuCyte live-cell analysis system was supported by shared equipment funds provided by the Sylvester Comprehensive Cancer Center. This work was funded by National Institutes of Health (NIH) grant CA136387 to E.A.M., grants GM115342 and CA200676 to S.L., grant CA250074 to E.C., and National Cancer Institute (NCI) diversity supplement R01CA136387-09S1 to O.M.-S. Clinical trial AMC066/A5263 was supported by AIDS Malignancy Consortium (AMC) grant U01 CA121947 from the NCI and the AIDS Clinical Trials Group (ACTG) awards UM1 AI068634, UM1 AI068636, and UM1 AI106701 from the National Institute of Allergy and Infectious Diseases (NIAID) of the NIH. The content is solely the responsibility of the authors and does not necessarily represent the official views of the NIH.

#### AUTHOR CONTRIBUTIONS

Conceptualization, O.M.-S., E.A.M., and S.L.; Methodology, O.M.-S., M.B., J.N., J.M.H., R.E.V., J.J.D.H., and P.R.T.; Investigation, O.M.-S., M.B., P.R.T., J.N., and R.E.V.; Resources, E.A.M. and S.L.; Data Analysis, O.M.-S., M.B., J.N., P.R.T., E.A.M., and S.L.; Writing – Original Draft, O.M.-S. and E.A.M.; Writing – Review & Editing, O.M.-S., J.N., J.J.D.H., P.R.T., E.A.M., M.B., and S.L.; Histopathological Specimen Examination & Immunohistochemistry Interpretation of AIDS-KS Lesions, E.C.; Supervision, E.A.M.

#### DECLARATION OF INTERESTS

The authors declare no competing interests

Received: April 30, 2021

Revised: May 19, 2021

Accepted: November 29, 2021

Published: December 28, 2021

#### REFERENCES

Arias, C., Walsh, D., Harbell, J., Wilson, A.C., and Mohr, I. (2009). Activation of host translational control pathways by a viral developmental switch. *PLoS Pathog.* *5*, e1000334.

Bojkova, D., Klann, K., Koch, B., Widera, M., Krause, D., Ciesek, S., Cinatl, J., and Munch, C. (2020). Proteomics of SARS-CoV-2-infected host cells reveals therapy targets. *Nature* *583*, 469–472.

Boyne, J.R., Jackson, B.R., Taylor, A., Macnab, S.A., and Whitehouse, A. (2010). Kaposi's sarcoma-associated herpesvirus ORF57 protein interacts with PYM to enhance translation of viral intronless mRNAs. *EMBO J.* *29*, 1851–1864.

Cai, Q.L., Knight, J.S., Verma, S.C., Zald, P., and Robertson, E.S. (2006). E655 ubiquitin complex is recruited by KSHV latent antigen LANA for degradation of the VHL and p53 tumor suppressors. *PLoS Pathog.* *2*, e116.

Cai, Q., Murakami, M., Si, H., and Robertson, E.S. (2007). A potential alpha-helix motif in the amino terminus of LANA encoded by Kaposi's sarcoma-associated herpesvirus is critical for nuclear accumulation of HIF-1alpha in normoxia. *J. Virol.* *81*, 10413–10423.

Carroll, P.A., Kenerson, H.L., Yeung, R.S., and Lagunoff, M. (2006). Latent Kaposi's sarcoma-associated herpesvirus infection of endothelial cells activates hypoxia-induced factors. *J. Virol.* *80*, 10802–10812.

Catrina, S.B., Botusan, I.R., Rantanen, A., Catrina, A.I., Pyakurel, P., Savu, O., Axelson, M., Biberfeld, P., Poellinger, L., and Brismar, K. (2006). Hypoxia-inducible factor-1alpha and hypoxia-inducible factor-2alpha are expressed in kaposi sarcoma and modulated by insulin-like growth factor-I. *Clin. Cancer Res.* *12*, 4506–4514.

Cavallin, L.E., Goldschmidt-Clermont, P., and Mesri, E.A. (2014). Molecular and cellular mechanisms of KSHV oncogenesis of Kaposi's sarcoma associated with HIV/AIDS. *PLoS Pathog.* *10*, e1004154.

Cavallin, L.E., Ma, Q., Naipauer, J., Gupta, S., Kurian, M., Locatelli, P., Romanelli, P., Nadji, M., Goldschmidt-Clermont, P.J., and Mesri, E.A. (2018). KSHV-induced ligand mediated activation of PDGF receptor-alpha drives Kaposi's sarcomagenesis. *PLoS Pathog.* *14*, e1007175.

Cesarman, E., Damania, B., Krown, S.E., Martin, J., Bower, M., and Whitty, D. (2019). Kaposi sarcoma. *Nat. Rev. Dis. Primers* *5*, 9.

Chapat, C., Jafarnejad, S.M., Matta-Camacho, E., Hesketh, G.G., Gelbart, I.A., Attig, J., Gkogkas, C.G., Alain, T., Stern-Ginossar, N., Fabian, M.R., et al. (2017). Cap-binding protein 4EHP effects translation silencing by microRNAs. *Proc. Natl. Acad. Sci. U S A* *114*, 5425–5430.

Cockman, M.E., Masson, N., Mole, D.R., Jaakkola, P., Chang, G.W., Clifford, S.C., Maher, E.R., Pugh, C.W., Ratcliffe, P.J., and Maxwell, P.H. (2000). Hypoxia inducible factor-alpha binding and ubiquitylation by the von Hippel-Lindau tumor suppressor protein. *J. Biol. Chem.* *275*, 25733–25741.

Davis, D.A., Rinderknecht, A.S., Zoetewij, J.P., Aoki, Y., Read-Connole, E.L., Tosato, G., Blauvelt, A., and Yarchoan, R. (2001). Hypoxia induces lytic replication of Kaposi sarcoma-associated herpesvirus. *Blood* *97*, 3244–3250.

Dittmer, D.P., and Damania, B. (2016). Kaposi sarcoma-associated herpesvirus: immunobiology, oncogenesis, and therapy. *J. Clin. Invest.* *126*, 3165–3175.

Duette, G., Pereyra Gerber, P., Rubione, J., Perez, P.S., Landay, A.L., Crowe, S.M., Liao, Z., Witwer, K.W., Holgado, M.P., Salido, J., et al. (2018). Induction of HIF-1alpha by HIV-1 infection in CD4+ T cells promotes viral replication and drives extracellular vesicle-mediated inflammation. *MBio* *9*, e00757-18.

Ganem, D. (2010). KSHV and the pathogenesis of Kaposi sarcoma: listening to human biology and medicine. *J. Clin. Invest.* *120*, 939–949.

Golas, G., Alonso, J.D., and Toth, Z. (2019). Characterization of de novo lytic infection of dermal lymphatic microvascular endothelial cells by Kaposi's sarcoma-associated herpesvirus. *Virology* *536*, 27–31.

Gomes, S.A., Rangel, E.B., Premer, C., Dulce, R.A., Cao, Y., Florea, V., Balkan, W., Rodrigues, C.O., Schally, A.V., and Hare, J.M. (2013). S-nitrosoglutathione reductase (GSNOR) enhances vasculogenesis by mesenchymal stem cells. *Proc. Natl. Acad. Sci. U S A* *110*, 2834–2839.

Guo, Y., Meng, X., Ma, J., Zheng, Y., Wang, Q., Wang, Y., and Shang, H. (2014). Human papillomavirus 16 E6 contributes HIF-1alpha induced Warburg effect by attenuating the VHL-HIF-1alpha interaction. *Int. J. Mol. Sci.* *15*, 7974–7986.

Haque, M., and Kousoulas, K.G. (2019). The Kaposi's sarcoma-associated herpesvirus ORF34 protein interacts and stabilizes HIF-2alpha via binding to the HIF-2alpha bHLH and PAS domains. *J. Virol.* *93*, e00764-19.

Haque, M., Davis, D.A., Wang, V., Widmer, I., and Yarchoan, R. (2003). Kaposi's sarcoma-associated herpesvirus (human herpesvirus 8) contains hypoxia response elements: relevance to lytic induction by hypoxia. *J. Virol.* *77*, 6761–6768.

Haque, M., Wang, V., Davis, D.A., Zheng, Z.M., and Yarchoan, R. (2006). Genetic organization and hypoxic activation of the Kaposi's sarcoma-associated herpesvirus ORF34-37 gene cluster. *J. Virol.* *80*, 7037–7051.

Ho, J.J.D., and Lee, S. (2016). A cap for every occasion: alternative eIF4F complexes. *Trends Biochem. Sci.* *41*, 821–823.

Ho, J.J.D., Wang, M., Audas, T.E., Kwon, D., Carlsson, S.K., Timpano, S., Evangelou, S.L., Brothers, S., Gonzalzo, M.L., Krieger, J.R., et al. (2016). Systemic reprogramming of translation efficiencies on oxygen stimulus. *Cell Rep.* *14*, 1293–1300.

- Ho, J.J.D., Balukoff, N.C., Theodoridis, P.R., Wang, M., Krieger, J.R., Schatz, J.H., and Lee, S. (2020). A network of RNA-binding proteins controls translation efficiency to activate anaerobic metabolism. *Nat. Commun.* **11**, 2677.
- Jackson, R.J. (2013). The current status of vertebrate cellular mRNA IRESs. *Cold Spring Harb. Perspect. Biol.* **5**, a011569.
- Jafarnejad, S.M., Chapat, C., Matta-Camacho, E., Gelbart, I.A., Hesketh, G.G., Arguello, M., Garzia, A., Kim, S.H., Attig, J., Shapiro, M., et al. (2018). Translational control of ERK signaling through miRNA/4EHP-directed silencing. *eLife* **7**, e35034.
- Jham, B.C., Ma, T., Hu, J., Chaisuparat, R., Friedman, E.R., Pandolfi, P.P., Schneider, A., Sodhi, A., and Montaner, S. (2011). Amplification of the angiogenic signal through the activation of the TSC/mTOR/HIF axis by the KSHV vGPCR in Kaposi's sarcoma. *PLoS ONE* **6**, e19103.
- Koon, H.B., Krown, S.E., Lee, J.Y., Honda, K., Rapisuwon, S., Wang, Z., Aboulafia, D., Reid, E.G., Rudek, M.A., Dezube, B.J., and Noy, A. (2014). Phase II trial of imatinib in AIDS-associated Kaposi's sarcoma: AIDS Malignancy Consortium Protocol 042. *J. Clin. Oncol.* **32**, 402–408.
- Krown, S.E., Roy, D., Lee, J.Y., Dezube, B.J., Reid, E.G., Venkataraman, R., Han, K., Cesarman, E., and Dittmer, D.P. (2012). Rapamycin with antiretroviral therapy in AIDS-associated Kaposi sarcoma: an AIDS Malignancy Consortium study. *J. Acquir. Immune Defic. Syndr.* **59**, 447–454.
- Lee, M.S., Yuan, H., Jeon, H., Zhu, Y., Yoo, S., Shi, S., Krueger, B., Renne, R., Lu, C., Jung, J.U., and Gao, S.J. (2016). Human mesenchymal stem cells of diverse origins support persistent infection with Kaposi's sarcoma-associated herpesvirus and manifest distinct angiogenic, invasive, and transforming phenotypes. *MBio* **7**, e02109–15.
- Lenarcic, E.M., Ziehr, B., De Leon, G., Mitchell, D., and Moorman, N.J. (2014). Differential role for host translation factors in host and viral protein synthesis during human cytomegalovirus infection. *J. Virol.* **88**, 1473–1483.
- Li, Y., Zhong, C., Liu, D., Yu, W., Chen, W., Wang, Y., Shi, S., and Yuan, Y. (2018). Evidence for Kaposi sarcoma originating from mesenchymal stem cell through KSHV-induced mesenchymal-to-endothelial transition. *Cancer Res.* **78**, 230–245.
- Liu, L., Cash, T.P., Jones, R.G., Keith, B., Thompson, C.B., and Simon, M.C. (2006). Hypoxia-induced energy stress regulates mRNA translation and cell growth. *Mol. Cell* **21**, 521–531.
- López-Rodríguez, D.M., Kirillov, V., Krug, L.T., Mesri, E.A., and Andreansky, S. (2019). A role of hypoxia-inducible factor 1 alpha in murine gammaherpesvirus 68 (MHV68) lytic replication and reactivation from latency. *PLoS Pathog.* **15**, e1008192.
- Mesri, E.A., Cesarman, E., and Boshoff, C. (2010). Kaposi's sarcoma and its associated herpesvirus. *Nat. Rev. Cancer* **10**, 707–719.
- Mesri, E.A., Feitelson, M.A., and Munger, K. (2014). Human viral oncogenesis: a cancer hallmarks analysis. *Cell Host Microbe* **15**, 266–282.
- Morita, M., Ler, L.W., Fabian, M.R., Siddiqui, N., Mullin, M., Henderson, V.C., Alain, T., Fonseca, B.D., Karashchuk, G., Bennett, C.F., et al. (2012). A novel 4EHP-GIGYF2 translational repressor complex is essential for mammalian development. *Mol. Cell. Biol.* **32**, 3585–3593.
- Myong, J., and Ganem, D. (2011). Generation of a doxycycline-inducible KSHV producer cell line of endothelial origin: maintenance of tight latency with efficient reactivation upon induction. *J. Virol. Methods* **174**, 12–21.
- Naipauer, J., Rosario, S., Gupta, S., Premer, C., Méndez-Solís, O., Schlesinger, M., Ponzinibbio, V., Jain, V., Gay, L., Renne, R., et al. (2019). PDGFRA defines the mesenchymal stem cell Kaposi's sarcoma progenitors by enabling KSHV oncogenesis in an angiogenic environment. *PLoS Pathog.* **15**, e1008221.
- Nakazawa, M.S., Eisinger-Mathason, T.S., Sadri, N., Ochocki, J.D., Gade, T.P., Amin, R.K., and Simon, M.C. (2016). Epigenetic re-expression of HIF-2 $\alpha$  suppresses soft tissue sarcoma growth. *Nat. Commun.* **7**, 10539.
- Park, S.K., Dadak, A.M., Haase, V.H., Fontana, L., Giaccia, A.J., and Johnson, R.S. (2003). Hypoxia-induced gene expression occurs solely through the action of hypoxia-inducible factor 1alpha (HIF-1alpha): role of cytoplasmic trapping of HIF-2alpha. *Mol. Cell. Biol.* **23**, 4959–4971.
- Persson, C.U., von Stedingk, K., Fredlund, E., Bexell, D., Pålman, S., Wigerup, C., and Mohlin, S. (2020). ARNT-dependent HIF-2 transcriptional activity is not sufficient to regulate downstream target genes in neuroblastoma. *Exp. Cell Res.* **388**, 111845.
- Pringle, E.S., Robinson, C.A., and McCormick, C. (2019). Kaposi's sarcoma-associated herpesvirus lytic replication interferes with mTORC1 regulation of autophagy and viral protein synthesis. *J. Virol.* **93**, e00854–19.
- Ren, L., Zhang, W., Han, P., Zhang, J., Zhu, Y., Meng, X., Zhang, J., Hu, Y., Yi, Z., and Wang, R. (2019). Influenza A virus (H1N1) triggers a hypoxic response by stabilizing hypoxia-inducible factor-1 $\alpha$  via inhibition of proteasome. *Virology* **530**, 51–58.
- Rosario, S.A., Santiago, G.E., Mesri, E.A., and Verdun, R.E. (2018). Kaposi's sarcoma-associated herpesvirus-encoded viral IL-6 (vIL-6) enhances immunoglobulin class-switch recombination. *Front. Microbiol.* **9**, 3119.
- Shin, Y.C., Joo, C.H., Gack, M.U., Lee, H.R., and Jung, J.U. (2008). Kaposi's sarcoma-associated herpesvirus viral IFN regulatory factor 3 stabilizes hypoxia-inducible factor-1 alpha to induce vascular endothelial growth factor expression. *Cancer Res.* **68**, 1751–1759.
- Shrestha, P., Davis, D.A., Veeranna, R.P., Carey, R.F., Viollet, C., and Yarchoan, R. (2017). Hypoxia-inducible factor-1 alpha as a therapeutic target for primary effusion lymphoma. *PLoS Pathog.* **13**, e1006628.
- Sodhi, A., Montaner, S., Patel, V., Zohar, M., Bais, C., Mesri, E.A., and Gutkind, J.S. (2000). The Kaposi's sarcoma-associated herpes virus G protein-coupled receptor up-regulates vascular endothelial growth factor expression and secretion through mitogen-activated protein kinase and p38 pathways acting on hypoxia-inducible factor 1alpha. *Cancer Res.* **60**, 4873–4880.
- Sodhi, A., Chaisuparat, R., Hu, J., Ramsdell, A.K., Manning, B.D., Sausville, E.A., Sawai, E.T., Molinolo, A., Gutkind, J.S., and Montaner, S. (2006). The TSC2/mTOR pathway drives endothelial cell transformation induced by the Kaposi's sarcoma-associated herpesvirus G protein-coupled receptor. *Cancer Cell* **10**, 133–143.
- Stallone, G., Schena, A., Infante, B., Di Paolo, S., Loverre, A., Maggio, G., Raniere, E., Gesualdo, L., Schena, F.P., and Grandaliano, G. (2005). Sirolimus for Kaposi's sarcoma in renal-transplant recipients. *N. Engl. J. Med.* **352**, 1317–1323.
- Stern-Ginossar, N., Thompson, S.R., Mathews, M.B., and Mohr, I. (2019). Translational control in virus-infected cells. *Cold Spring Harb. Perspect. Biol.* **11**, a033001.
- Sternbach, G., and Varon, J. (1995). Moritz Kaposi: idiopathic pigmented sarcoma of the skin. *J. Emerg. Med.* **13**, 671–674.
- Talks, K.L., Turley, H., Gatter, K.C., Maxwell, P.H., Pugh, C.W., Ratcliffe, P.J., and Harris, A.L. (2000). The expression and distribution of the hypoxia-inducible factors HIF-1 $\alpha$  and HIF-2 $\alpha$  in normal human tissues, cancers, and tumor-associated macrophages. *Am. J. Pathol.* **157**, 411–421.
- Tian, H., McKnight, S.L., and Russell, D.W. (1997). Endothelial PAS domain protein 1 (EPAS1), a transcription factor selectively expressed in endothelial cells. *Genes Dev.* **11**, 72–82.
- Timpano, S., and Uniacke, J. (2016). Human Cells cultured under physiological oxygen utilize two cap-binding proteins to recruit distinct mRNAs for translation. *J. Biol. Chem.* **291**, 10772–10782.
- Tomlinson, C.C., and Damania, B. (2004). The K1 protein of Kaposi's sarcoma-associated herpesvirus activates the Akt signaling pathway. *J. Virol.* **78**, 1918–1927.
- Uniacke, J., Holterman, C.E., Lachance, G., Franovic, A., Jacob, M.D., Fabian, M.R., Payette, J., Holcik, M., Pause, A., and Lee, S. (2012). An oxygen-regulated switch in the protein synthesis machinery. *Nature* **486**, 126–129.
- Uniacke, J., Perera, J.K., Lachance, G., Francisco, C.B., and Lee, S. (2014). Cancer cells exploit eIF4E2-directed synthesis of hypoxia response proteins to drive tumor progression. *Cancer Res.* **74**, 1379–1389.
- Viollet, C., Davis, D.A., Tekeste, S.S., Reczko, M., Ziegelbauer, J.M., Pezzella, F., Ragoussis, J., and Yarchoan, R. (2017). RNA sequencing reveals that Kaposi sarcoma-associated herpesvirus infection mimics hypoxia gene expression signature. *PLoS Pathog.* **13**, e1006143.



- von Stechow, L., Typas, D., Carreras Puigvert, J., Oort, L., Siddappa, R., Pines, A., Vrieling, H., van de Water, B., Mullenders, L.H., and Danen, E.H. (2015). The E3 ubiquitin ligase ARIH1 protects against genotoxic stress by initiating a 4EHP-mediated mRNA translation arrest. *Mol. Cell. Biol.* **35**, 1254–1268.
- Wakisaka, N., Kondo, S., Yoshizaki, T., Murono, S., Furukawa, M., and Pagano, J.S. (2004). Epstein-Barr virus latent membrane protein 1 induces synthesis of hypoxia-inducible factor 1 alpha. *Mol. Cell. Biol.* **24**, 5223–5234.
- Walsh, D., and Mohr, I. (2011). Viral subversion of the host protein synthesis machinery. *Nat. Rev. Microbiol.* **9**, 860–875.
- Walsh, D., Mathews, M.B., and Mohr, I. (2013). Tinkering with translation: protein synthesis in virus-infected cells. *Cold Spring Harb. Perspect. Biol.* **5**, a012351.
- Wang, G.L., Jiang, B.H., Rue, E.A., and Semenza, G.L. (1995). Hypoxia-inducible factor 1 is a basic-helix-loop-helix-PAS heterodimer regulated by cellular O<sub>2</sub> tension. *Proc. Natl. Acad. Sci. U S A* **92**, 5510–5514.
- Wang, L., Dittmer, D.P., Tomlinson, C.C., Fakhari, F.D., and Damania, B. (2006). immortalization of primary endothelial cells by the K1 protein of Kaposi's sarcoma-associated herpesvirus. *Cancer Res.* **66**, 3658–3666.
- Yi, T., Papadopoulos, E., Hagner, P.R., and Wagner, G. (2013). Hypoxia-inducible factor-1 $\alpha$  (HIF-1 $\alpha$ ) promotes cap-dependent translation of selective mRNAs through up-regulating initiation factor eIF4E1 in breast cancer cells under hypoxia conditions. *J. Biol. Chem.* **288**, 18732–18742.
- Yogev, O., Lagos, D., Enver, T., and Boshoff, C. (2014). Kaposi's sarcoma herpesvirus microRNAs induce metabolic transformation of infected cells. *PLoS Pathog.* **10**, e1004400.
- Zhang, L., Zhu, C., Guo, Y., Wei, F., Lu, J., Qin, J., Banerjee, S., Wang, J., Shang, H., Verma, S.C., et al. (2014). Inhibition of KAP1 enhances hypoxia-induced Kaposi's sarcoma-associated herpesvirus reactivation through RBP-Jk. *J. Virol.* **88**, 6873–6884.

STAR★METHODS

KEY RESOURCES TABLE

REAGENT or RESOURCE	SOURCE	IDENTIFIER
<b>Antibodies</b>		
Human HIF2 $\alpha$ (WB and IF)	Bethyl Laboratories	Cat.# A700-003, Clone# BL-95-1A2; RRID:AB_2631884
KSHV K8.1 (WB and IF)	Santa Cruz Biotechnology	Cat.# sc-65446; RRID:AB_831825
KSHV ORF57	Santa Cruz Biotechnology	Cat.# sc-135746; RRID:AB_2011972
Calnexin	Santa Cruz Biotechnology	Cat.# sc-23954; RRID:AB_626783
Alexa 647 Goat anti-mouse IgG	Invitrogen	Cat.# A32728; RRID:AB_2633277
Alexa 555 Goat anti-rabbit IgG	Invitrogen	Cat.# A21429; RRID:AB_2535850
Human HIF1 $\alpha$	Bethyl Laboratories	Cat.# A700-001, Clone# BL-124-3F7; RRID:AB_2631882
Human $\beta$ -actin	Sigma	Cat.# A5441, Clone# AC-15; RRID:AB_476744
Human cyclin D1	Santa Cruz Biotechnology	Cat.# sc-8396; RRID:AB_627344
KSHV LANA	Abcam	Cat.# ab4103, Clone# LN53; RRID:AB_304278
KSHV ORF45	ThermoFisher Scientific	Cat.# MA5-14769, Clone# 2D4A5; RRID:AB_10999794
Human HIF1 $\beta$	BD Laboratories	Cat.# 611078; RRID:AB_398391
Human PDGFA	Santa Cruz Biotechnology	Cat.# sc-9974; RRID:AB_2161916
Human PDGFB	Santa Cruz Biotechnology	Cat.# sc-365805; RRID:AB_10848458
KSHV gB	ThermoFisher Scientific	Cat.# PA5-19852; RRID:AB_10983284
KSHV RTA	ABBIOTEC	Cat.# 251345; RRID:AB_10643806
Human PDGFRA	R&D systems	Cat.# AF1062-SP; RRID:AB_2236897
Human p-PDGFR $\alpha$	R&D systems	Cat.# AF2114; RRID:AB_416551
Human eIF4E2	GeneTex	Cat.# GTX103977; RRID:AB_2036842
Human eIF4E1	Santa Cruz Biotechnology	Cat.# sc-9976; RRID:AB_627502
HHV-8 ORF73 (Immunohistochemistry)	Leica	Cat.# PA0050
HHV-8 K8.1 (Immunohistochemistry)	Advanced Biotechnologies	Cat.# 13-213-100, Clone# 2A3; RRID:AB_1929220
HIF2 $\alpha$ (Immunohistochemistry)	Bethyl Laboratories	Cat.#A700-003, Clone# BL-95-1A2; RRID:AB_2631884
eIF4G3	GeneTex	Cat.# GTX118109; RRID:AB_11167995
RBM4	Santa Cruz Biotechnology	Cat.# sc-373852; RRID:AB_10986005
HA	Santa Cruz Biotechnology	Cat.# sc-7392; RRID:AB_2894930
eIF4G1	Novus Biologicals	Cat.# NB100-268; RRID:AB_10001835
<b>Bacterial and virus strains</b>		
rKSHV.219	iSLK.KSHV219 cells provided by Dr. Don Ganem	Previously described in (Rosario et al., 2018)
<b>Biological samples</b>		
KS biopsies	ACTG# NCT01435018	PMID 32145827
<b>Chemicals, peptides, and recombinant proteins</b>		
MG132	Sigma	Cat.# C2211
SuperSignal West Pico PLUS Chemiluminescent Substrate	ThermoFisher Scientific	Cat.# 34577
Actinomycin D	ThermoFisher Scientific	Cat.# A7592
Cyclohexamide	VWR Scientific	Cat.# 94271
Puromycin	GIBCO	Cat.# A11138-03
G418	Sigma	Cat.# G8168
Hygromycin B	Invitrogen	Cat.# 10687-010
Endothelial Cell Growth Factor (ECGF) + Heparin	ReliaTech	Cat.# 300-090H
Endothelial Cell Growth Supplement(ECGS)	Sigma-Aldrich	Cat.# E2759

(Continued on next page)

**Continued**

REAGENT or RESOURCE	SOURCE	IDENTIFIER
Insulin/transferrin/selenium	Sigma-Aldrich	Cat.# I3146
MEM Vitamin	Sigma-Aldrich	Cat.# M6895
Polybrene	Millipore	Cat.# TR-1003-G
Doxycycline	Sigma	Cat.# D9891
RIPA lysis buffer	ThermoFisher Scientific	Cat.# 89900
Protease inhibitors	Sigma	Cat.# P8340
Phosphatase inhibitor Cocktail 2	Sigma	Cat.# P5726
Phosphatase inhibitor Cocktail 3	Sigma	Cat.# P0044
Laemmli buffer	Biorad	Cat.# 161-0747
SYBR green PCR master mix	Quanta Biosciences	Cat.# 95073-012
Proteinase K	Ambion	Cat.# AM2546
RNaseOut	Invitrogen	Cat.# 10777-019
IP buffer	ThermoFisher Scientific	Cat.# 87788
m <sup>7</sup> GTP agarose beads	Jena Biosciences	Cat.# AC-155S
Blank agarose beads	Jena Biosciences	Cat.# AC-001S
Paraformaldehyde (PFA)	Alfa Aesar	Cat.# 43368
Phenol:chloroform:isoamyl alcohol	Fisher Scientific	Cat.# BP17541
Chloroform	Fisher Scientific	Cat.# BP1145
PBS (RNase free)	Fisher Scientific	Cat.# BP2438-4
Rabbit mAb IgG Magnetic Bead Conjugate	Cell Signaling	Cat.# 8726
HA-Tag Rabbit mAb Magnetic Bead Conjugate	Cell Signaling	Cat.# 11846
<b>Critical commercial assays</b>		
BCA protein assay	ThermoFisher Scientific	Cat.# 23227
VivaFix 410/450	BioRad	Cat.# 135-1112
RNeasy Kit	QIAGEN	Cat.# 74104
RNase-Free DNase kit	QIAGEN	Cat.# 79254
Amplification grade DNase I	Sigma	Cat.# AMPD1
Im-PromII Reverse Transcriptase	Promega	Cat.# A3802
Lipofectamine 2000	Life Technologies	Cat.# 11668-027
Lipofectamine RNAiMAX reagent	Life Technologies	Cat.# 13778-075
Magna RIP RNA-Binding Protein Immunoprecipitation Kit	Millipore	Cat.# 17-700
VEGF-A ELISA kit	Cusabio	Cat.# CSB-E11718h
<b>Experimental models: Cell lines</b>		
iSLK.KSHV219 cells	Provided by Dr. Don Ganem	Previously described in ( <a href="#">Myoung and Ganem, 2011</a> )
iSLK.KSHVnegative cells	Provided by Dr. Don Ganem	N/A
HEK-AD293 cells	Agilent	Cat.# 240085, RRID# CVCL_9804
<b>Experimental models: Organisms/strains</b>		
Human Mesenchymal Stem Cells	Provided by Dr. Joshua Hare	Previously described in ( <a href="#">Gomes et al., 2013</a> )
<b>Oligonucleotides</b>		
Primers for qRT-PCR used in this study	Sigma	<a href="#">Table S1</a>
Control siRNA	Dharmacon	Cat.#D-001206-13-05
Human eIF4E2 siRNA	Dharmacon	Cat.# M-019870-01-0005
Human eIF4E1 siRNA	Dharmacon	Cat.# M-003884-03-0005
Human HIF2 $\alpha$ siRNA	Dharmacon	Cat.# M-004814-01-0005
Human HIF1 $\beta$ siRNA	Dharmacon	Cat.# M-007207-01-0005

(Continued on next page)

**Continued**

REAGENT or RESOURCE	SOURCE	IDENTIFIER
<b>Recombinant DNA</b>		
eIF4E2-HA	Addgene	Cat.# 17344
eIF4E1-HA	Addgene	Cat.# 17343
HIF2 $\alpha$ -HA	Addgene	Cat.# 18950
<b>Software and algorithms</b>		
PowerGene 9600 Plus Real-time PCR system	ATILA BioSystems	<a href="https://atilabiosystems.com/our-products/linegene-9600-plus-real-time-pcr-system/">https://atilabiosystems.com/our-products/linegene-9600-plus-real-time-pcr-system/</a>
Peakchart Software (polysome profiling)	Brandel	<a href="http://www.brandel.com/fractgradient.html">http://www.brandel.com/fractgradient.html</a>
IncuCyte Zoom Software	Essen Bioscience	<a href="https://www.essenbioscience.com/updates/IncuCyteZoom/IncuCyteZOOM2018AGuiSetup/">https://www.essenbioscience.com/updates/IncuCyteZoom/IncuCyteZOOM2018AGuiSetup/</a>
LASX software	Leica	<a href="https://www.leica-microsystems.com/products/microscope-software/p/leica-las-x-ls/downloads/">https://www.leica-microsystems.com/products/microscope-software/p/leica-las-x-ls/downloads/</a>
ImageJ for quantifying immunoblot bands	ImageJ	<a href="https://imagej.nih.gov/ij/download.html">https://imagej.nih.gov/ij/download.html</a>

**RESOURCE AVAILABILITY**

**Lead contact**

Further information and requests for resources or reagents should be directed and will be fulfilled by Enrique A. Mesri ([emesri@med.miami.edu](mailto:emesri@med.miami.edu)).

**Materials availability**

This study did not generate new unique reagents.

**Data and code availability**

- All data reported in this paper will be shared by the lead contact upon request.
- This paper does not report original code.
- Any additional information required to reanalyze the data reported in this paper is available from the lead contact upon request.

**EXPERIMENTAL MODEL AND SUBJECT DETAILS**

**Cell lines**

iSLK.KSHV219 cells (human clear cell renal carcinoma- male; RRID: CVCL-9569), iSLK-KSHVnegative cells (human clear cell renal carcinoma- male; RRID: CVCL-9569) and HEK-AD293 cells (human fetus transformed cell line- female; RRID:CVCL\_9804) were cultured in Dulbecco's modified eagle medium (DMEM/Corning) containing 10% FBS (Gemini Bio-Products) and 1% penicillin-streptomycin (GIBCO) at 37°C and 5% CO<sub>2</sub>. As previously described, these cells were selected with 10  $\mu$ g/mL of puromycin (GIBCO), 50  $\mu$ g/mL of G418 (Sigma), and only for the infected cells 50  $\mu$ g/mL of Hygromycin B (Invitrogen) (Myoung and Ganem, 2011).

**Primary cell cultures**

Primary Human MSCs (human bone marrow iliac crest biopsy-female; provided by Dr. Joshua Hare), isolated as previously described by (Gomes et al., 2013), were maintained either in MSC media: Minimum essential medium ( $\alpha$ MEM/Invitrogen) supplemented with 20% FBS (Atlanta Biologicals) and 1% penicillin-streptomycin or KS-like media: Dulbecco's modified eagle medium (DMEM/Corning) containing 30% FBS (Gemini Bio-Products), 0.2mg/mL Endothelial Cell Growth Factor (ECGF) (ReliaTech), 0.2  $\mu$ g/mL Endothelial Cell Growth Supplement (ECGS) (Sigma-Aldrich), 1.2  $\mu$ g/mL heparin (Sigma-Aldrich), insulin/transferrin/selenium (Invitrogen), 1% penicillin-streptomycin (GIBCO) and MEM vitamin (VWR Scientific) at 37°C and 5% CO<sub>2</sub> (Gomes et al., 2013; Naipauer et al., 2019).

**Human tissue samples**

Tissue samples from 10 human cases (age and gender were anonymized for research purposes) with Kaposi's Sarcoma from AIDS Clinical Trials Group (ACTG) (clinical trial # NCT01435018; PIMD32145827) were used. These cases were randomly and blindly selected based on KSHV K8.1 expression. Approval was obtained from the respective institutional IRBs (IRB approval # 9606000390) for use of all tissue specimens for biomarker analysis.



## METHOD DETAILS

### Transient RNA interference

iSLK.KSHV219, iSLK-KSHVnegative and human MSCs were transiently transfected prior reactivation and *de novo* rKSHV219 infection with small interfering RNA (siRNA) at a final concentration of 25 pmol/well using Lipofectamine RNAiMAX reagent (Life Technologies). All siRNAs were purchased from GE Dharmacon: control siRNA (D-001206-13-05) human eIF4E2 siRNA (M-019870-01-0005), human HIF2 $\alpha$  siRNA (M-004814-01-0005), human HIF1 $\beta$  siRNA (M-007207-01-0005), and human eIF4E1 siRNA (M-003884-03-0005).

### Lytic Induction and AD293 TCID<sub>50</sub>

24 h post transient siRNA transfection, iSLK.KSHV219 cells were induced at 60% confluency with 1  $\mu$ g/ $\mu$ L doxycycline (Sigma). After 24 to 72 h of induction, cell-free virus containing supernatants were collected and after a serial dilution were used to *de novo* infect HEK-AD293 pre-treated with 8  $\mu$ g/mL of polybrene (Millipore) by spinoculation at 700 x g for 60 min at 30°C. 72 h post infection, infectious virion production was measured by counting the GFP+ HEK-AD293 by flow cytometry to determine the 50% tissue culture infective dose (TCID<sub>50</sub>) (1 GFP+ HEK-AD293 = 1 infectious KSHV virion). In the case of productively infected hMSCs, infectious viral particles in supernatants were collected 72 h post *de novo* infection and were used to infect HEK-AD293 as described above.

### hMSCs *de novo* infection with rKSHV219

72 h post-siRNA transfection, human MSCs were infected with rKSHV219 by spinoculation at 700 x g for 60 min at 30°C in the presence of 8  $\mu$ g/mL of polybrene at multiplicity of infection (MOI) of 10. rKSHV219 was obtained as previously described (Rosario et al., 2018). Briefly, iSLK.KSHV219 cells were induced with 1mM sodium butyrate and 1  $\mu$ g/ $\mu$ L doxycycline to produce infectious KSHV virions. Cell-free virus-containing supernatants were then collected 96 h post-reativation. To obtain concentrated virus for infection of hMSCs, these supernatants were spun at 27,000 x g for 90 min at 4°C.

### Western blotting (WB)

RIPA lysis buffer (ThermoScientific) containing protease and phosphatase inhibitors (Sigma) was used to obtain protein lysates. These lysates were sonicated and centrifuged at 10,000 rpm for 10min to remove genomic DNA. Protein concentration was measured using BCA protein assay (ThermoScientific) prior Laemmli buffer (Bio-rad) containing  $\beta$ -mercaptoethanol addition. 20  $\mu$ g of protein was loaded and resolved in SDS-PAGE gel (Biorad). The gel was transferred to a PVDF membrane (BioRad) and blocked with 5% BSA (Sigma) for 1 h to reduce non-specific binding. Membranes were incubated with primary antibodies diluted in 5% BSA overnight. Monoclonal antibodies were used for human HIF1 $\alpha$  (Bethyl Laboratories), human HIF2 $\alpha$  (Bethyl Laboratories), human  $\beta$ -actin (Sigma), KSHV LANA (Abcam), KSHV ORF45 (ThermoFisher Scientific), KSHV K8.1 (Santa Cruz Biotechnology), KSHV ORF57 (Santa Cruz Biotechnology), human HIF1 $\beta$  (BD Laboratories), human cyclin D1 (Santa Cruz Biotechnology), human PDGFA (Santa Cruz Biotechnology), human PDGFB (Santa Cruz Biotechnology), Calnexin (Santa Cruz Biotechnology), RBM4 (Santa Cruz Biotechnology) and HA (Santa Cruz Biotechnology). Polyclonal antibodies were used for KSHV gB (ThermoFisher Scientific), KSHV RTA (ABBIOTEC), human PDGFRA (R&D Systems), human phospho-PDGFR $\alpha$  (R&D Systems), eIF4E2 (GeneTex), eIF4E1 (Santa Cruz Biotechnology), eIF4G1 (Novus Biologicals) and eIF4G3 (GeneTex). Protein bands were visualized using SuperSignal West Pico PLUS Chemiluminescent Substrate (ThermoScientific). The intensities of the western blot bands were measured using ImageJ software. 20 $\mu$ M of MG132 (Sigma) was used to rescue the proteins that were targeted to the proteasome for degradation, specifically cells were treated with MG132 6 h prior collection of protein lysates. For actinomycin D (ActD) and cycloheximide (CHX) treatment, reactivated cells after 48 h were treated with 1  $\mu$ g/mL of ActD and 10  $\mu$ g/mL of CHX.

### Flow cytometry

To measure the amount of infected (GFP+) and reactivated (GFP+/RFP+) iSLK.KSHV219, HEK-AD293 and hMSCs, cells were washed 2X with 1X PBS and fixed with 4% paraformaldehyde. For cell viability measurement, we used VivaFix 410/450 (BioRad #135-1112) per manufacturer instructions. Flow cytometry analysis was performed using Becton Dickinson LSR analyzer (BDBiosciences).

### Real-time quantitative PCR (RT-qPCR)

RNA was extracted from cells using RLT buffer (RNeasy Kit QIAGEN) containing  $\beta$ -mercaptoethanol or by phenol-chloroform extraction (Fisher Scientific) with ethanol precipitation. To remove DNA, samples were treated with RNase-Free DNase (QIAGEN) on columns for 25 min or amplification grade DNase I (Sigma) for 15 min at room temperature. RNA was reverse transcribed into cDNA using ImProm-II Reverse Transcriptase (Promega) as directed by manufacturer's protocol. Viral and host mRNAs were amplified using specific primers (Sigma, refer to Table S1) diluted in SYBR green PCR master mix (Quanta Biosciences). For detection, we used PowerGene 9600 Plus Real-time PCR system (ATILA BioSystems). Non-reverse transcriptase and water controls were used to confirm the absence of viral DNA and contamination in the samples. Actin was used as a housekeeping gene to perform  $\Delta\Delta$ CT method. The expression of host and viral genes was normalized to actin CT value and the difference between the host and viral

CT values with actin CT value was considered the  $\Delta$ CT value. The obtained  $\Delta$ CT values were then normalized to a given siControl sample ( $\Delta\Delta$ CT value) and the fold change was calculated using  $2^{-\Delta\Delta\text{CT}}$  formula. For the analysis of viral genes obtained after HIF2 $\alpha$  and eIF4E2/eIF4E1 RIPs and polysome profiling, HIF2 $\alpha$  and eIF4E2/eIF4E1 RIPs CT values were normalized to the input CT value that was obtained before performing the RIP, whereas, the CT values of each fractions obtained by polysomes profiling were normalized to the input RNA of each viral gene ( $\Delta$ CT value). The  $\Delta$ CT values of the RIPs were then normalized to IgG or empty control RIP to get the  $\Delta\Delta$ CT value. In the case of the  $\Delta$ CT values of oligosome and polysome fractions the normalization was relative to the  $\Delta$ CT value of the monosome fraction ( $\Delta\Delta$ CT value). The fold change was obtained using  $2^{-\Delta\Delta\text{CT}}$  formula.

### Polysome profiling

iSLK.KSHV219 cells were silenced as previously described and grown in 15-cm dishes to 95% confluency. mRNAs associated with monosomes, oligosomes and polysomes were collected as previously described (Timpano and Uniacke, 2016). Briefly, cells were treated with 0.2mg/mL cycloheximide (VWR Scientific) for 10min before harvesting to immobilized translating ribosomes. RNA lysis buffer [15 mM Tris-HCL (pH 7.4), 15mM MgCl<sub>2</sub>, 0.3 M NaCl, 1% Triton X-100, 0.2mg/mL cycloheximide and 200 units/mL RNaseOut (Invitrogen)] was used to collect immobilized translating ribosomes. Equal number of RNA from each condition were loaded onto a 10%–50% sucrose density gradient. The gradients were sedimented by centrifugation at 39,000 rpm for 90 min at 4°C and fractionated using Brandel BR-188 density gradient fractionation system. Peakchart software (Brandel) was used to get polysomes profiles. Each fraction was treated with proteinase K (Ambion) to obtain mRNAs using phenol-chloroform extraction with ethanol precipitation.

### RNA immunoprecipitation (RIP)

Before RIP procedure, iSLK.KSHV219 cells were treated with DOX for 24 h. In the case of eIF4E2-HA and eIF4E1-HA RIPs, cells were transfected 48 h prior DOX treatment with empty (pcDNA3), eIF4E2-HA and eIF4E1-HA (Addgene) plasmids using Lipofectamine 2000 (Life Technologies). Magna RIP RNA-Binding Protein Immunoprecipitation Kit (Millipore) was used to collect viral and/or host mRNAs associated with endogenous HIF2 $\alpha$ , eIF4E2-HA and eIF4E1-HA according to manufacturer's instructions.

### Cell proliferation assay (Incucyte)

Human MSCs were plated at 25,000 cells/well in 3 replicates and then silenced for 72 h. The silenced hMSCs were then infected with rKSHV219 by spinoculation at 700 x g for 60 min at 30°C and incubated in an Incucyte Zoom incubator (Essen Bioscience) to acquire green and red fluorescence images at 10 x magnification every 4 hours. To graph the results relative to the total number of cells in the well, the Incucyte Zoom software was used.

### Enzyme-linked immunosorbent assay (ELISA)

The amount of VEGF-A present in cell-free supernatants was measured using a Human VEGF-A ELISA kit per manufacturer's instructions (Cusabio).

### M<sup>7</sup>GTP pulldowns

iSLK.KSHV219 and iSLK-KSHVnegative were used to pulldown cap-binding complexes as previously described (Pringle et al., 2019). Briefly,  $2 \times 10^6$  cells were washed with 1X PBS and harvested with IP buffer (ThermoFisher Scientific) containing phosphatase and protease inhibitors (Sigma). Then, the lysates were centrifuged for 10 min at 10,000 rpm/4°C for elimination of cell debris. To remove non-specific protein binding to the agarose beads, the lysates were pre-cleared with blank agarose beads (Jena Bioscience) with rotation for 10min at 4°C. The blank beads were pelleted for 1min at 500 g for removal of non-specific binders and 5% of the supernatant was collected as protein input. The pre-cleared lysates were then incubated with m<sup>7</sup>GTP agarose beads (Jena Biosciences) at 4°C for 4 h with rotation. Lastly, the m<sup>7</sup>GTP beads were pelleted down, washed four times with IP buffer, resuspended in 50 $\mu$ L of 2X Laemmli (Bio-rad) containing  $\beta$ -mercaptoethanol (BME), boiled for 5 min at 90°C and finally resolved in a SDS-PAGE gel (Bio-rad). For the RNase treatment, after the 4 h incubation at 4°C the m<sup>7</sup>GTP beads were washed 4 times with IP buffer and then treated with RNase or left untreated for 20 min at 25°C with rotation. After RNase treatment, the beads were washed 4 additional times with IP buffer and then resuspended in 50  $\mu$ L of 2X Laemmli buffer containing BME, boiled for 5 min and resolved by SDS-PAGE gel.

### Protein immunoprecipitation (IP)

$2 \times 10^6$  iSLK.KSHV219 cells were transfected with eIF4E2-HA, eIF4E1-HA and HIF2 $\alpha$ -HA 24 h prior reactivation. Then, 24 h or 48 h post-reactivation, cells were washed with 1X PBS and harvested with IP buffer (ThermoFisher Scientific) containing phosphatase and protease inhibitors (Sigma). 5% of input sample was removed before IP. Then, IgG XP Isotype magnetic beads (Cell Signaling) and HA-conjugated magnetic beads (Cell Signaling) were added to the respective sample following manufacture's recommendation. The samples containing beads were rotated at 4°C for 6 h. Then beads were washed 4 times prior to RNase treatment. The beads were treated with RNase or left untreated for 20 min at 25°C with rotation. After RNase incubation, the beads were washed 4 additional times and resuspended in 50  $\mu$ L of 2X Laemmli buffer containing BME, boiled for 5 min and resolved in SDS-PAGE gel.

### Immunofluorescence (IF)

Latent and reactivated iSLK.KSHV 219 cells were washed 3 times with 1X PBS and then fixed with 4% paraformaldehyde (PFA) for 10min at room temperature (RT). For cell membrane permeabilization, cells were incubated with 0.05% Triton X-100 at RT for 5min. Then, cells were blocked with IFA blocking solution (1% BSA, 3.5% Goat Serum and 0.1% Tween 20 in 1X PBS) for 1 h at RT. The primary antibody was subsequently diluted in the blocking solution and incubated overnight at 4°C. Monoclonal antibodies were used for human HIF2 $\alpha$  (Bethyl Laboratories), KSHV K8.1 (Santa Cruz Biotechnology), KSHV ORF57 (Santa Cruz Biotechnology) and Calnexin (Santa Cruz Biotechnology). The next day, cells were washed 3 times with 1X PBS and incubated with Alexa 647 or Alexa 555 conjugated secondary antibodies (Invitrogen) diluted in blocking solution for 1 h at RT. Lastly, the stained cells were washed 3 times with 1X PBS, rinsed once with ddH<sub>2</sub>O and slides were mounted using prolong diamond antifade DAPI mounting solution (ThermoFisher Scientific). Samples were analyzed using a Leica DMI6000B microscope with LASX software (Leica).

### Immunohistochemistry of KS tumors

Ten cases were selected based on previous assessment for K8.1, to include seven positive cases and three negative cases. These cases had been previously stained by immunohistochemistry (IHC) for KSHV LANA and K8.1, as part of an AIDS Malignancy Consortium (AMC) and AIDS Clinical Trials Group (ACTG) clinical trial, AMC066/A5263 (NCT01435018; PMID 32145827), and HIF2 $\alpha$  IHC was added for this study. Immunophenotyping was performed on formalin-fixed, paraffin-embedded tissue sections on a Leica Bond III system using the standard protocol. Sections were pre-treated using heat-mediated antigen retrieval with Sodium-Citrate buffer (pH6, epitope retrieval solution 1) for 30 mins. The sections were then incubated with appropriate antibodies for 15 mins at room temperature and detected using an HRP-conjugated compact polymer system. 3,3'-Diaminobenzidine (DAB) was used as the chromogen. Sections were then counterstained with hematoxylin and mounted with micromount. The following antibodies were used for IHC: anti-LANA mouse monoclonal HHV-8 ORF73 (Leica, Catalog Number PA0050), anti-K8.1 mouse monoclonal (Advanced Biotechnologies, Clone 2A3, Catalog Number 13-213-100) and anti-HIF2 $\alpha$  rabbit monoclonal clone BL-95-1A2 (Bethyl Laboratories, Catalog Number A700-003).

### QUANTIFICATION AND STATISTICAL ANALYSIS

The statistical significance of all collected data was calculated using one-tailed unpaired Student's t test or 2-way ANOVA with Sidak's or Tukey's post-test using GraphPad Prism 9 software. A p value lower than 0.05 was indicated as significant. Values are expressed as means (n = 3)  $\pm$  standard deviation or as median (n = 3) with range. The number of replicates are indicated in the figure legends. Densitometry analysis of western blot bands was performed using ImageJ software as indicated in figure legends.

### ADDITIONAL RESOURCES

The KS samples were collected from individuals of a clinical trial register as: NCT01435018. Further information of this clinical trial can be found in: <https://clinicaltrials.gov/ct2/show/NCT01435018> and [https://www.thelancet.com/journals/lancet/article/PIIS0140-6736\(19\)33222-2/fulltext](https://www.thelancet.com/journals/lancet/article/PIIS0140-6736(19)33222-2/fulltext)

Cell Reports, Volume 37

## Supplemental information

### **Kaposi's sarcoma herpesvirus activates the hypoxia response to usurp HIF2 $\alpha$ -dependent translation initiation for replication and oncogenesis**

**Omayra Méndez-Solís, Mourad Bendjennat, Julian Naipauer, Phaedra R. Theodoridis, J.J. David Ho, Ramiro E. Verdun, Joshua M. Hare, Ethel Cesarman, Stephen Lee, and Enrique A. Mesri**



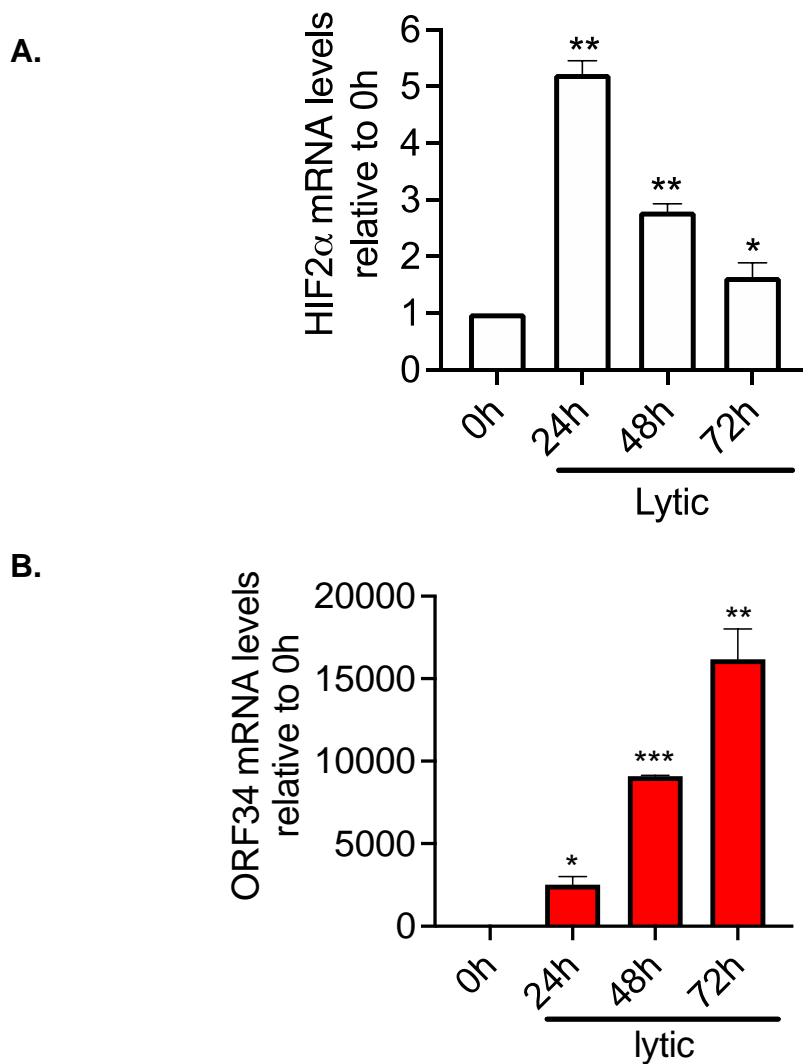


**Figure S1| HIF2 $\alpha$  and KSHV ORF34 mRNAs levels during KSHV lytic program, related to Figure 1. A)** HIF2 $\alpha$  mRNA levels in reactivated iSLK.KSHV219 cells relative to 0 h (before addition of DOX) measured by qRT-PCR (n=3) (mean $\pm$  SD, \*\* p< 0.0001, \* p< 0.05, Unpaired t test) **B)** Kinetics of KSHV ORF34 mRNAs levels during lytic replication, as in (A) mRNA levels were measured (n=3, mean $\pm$  SD, \*\*\* p< 0.0001, \*\* p< 0.01, \* p< 0.05, Unpaired t test).

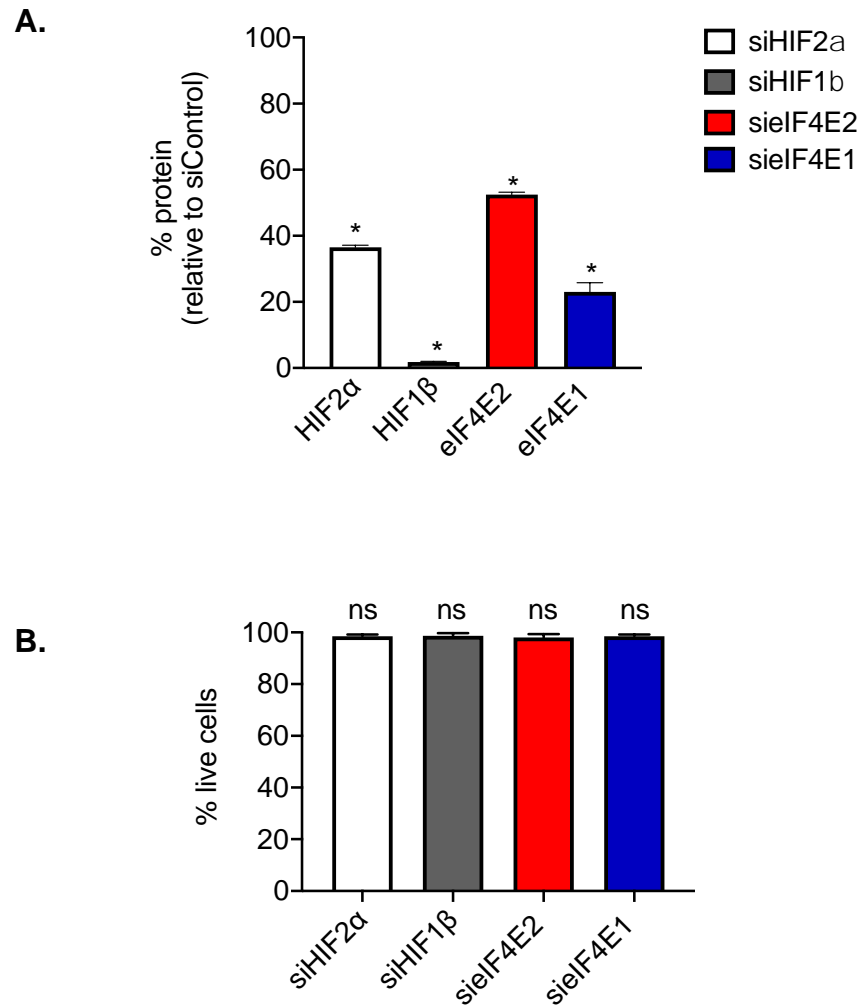


**Figure S2| Effects of Transient RNA interference in iSLK.KSHV219 cells, related to Figure 1 and Figure 2. A)** Silencing efficiency of siHIF2 $\alpha$ , siHIF1 $\beta$ , siEIF4E2, siEIF4E1. iSLK.KSHV219 cells were silenced prior to reactivation and the protein level of the target gene relative to siControl 24 h post silencing was calculated using ImageJ (n=3, mean $\pm$  SD, \* p < 0.001, unpaired t test). **B)** Percentage of live iSLK.KSHV219 cells that were silenced with siEIF4E2, siEIF4E1, siHIF2 $\alpha$  or siHIF1 $\beta$  for 72 h in normoxia (n=3, mean $\pm$  SD, ns= not significant, unpaired t test).

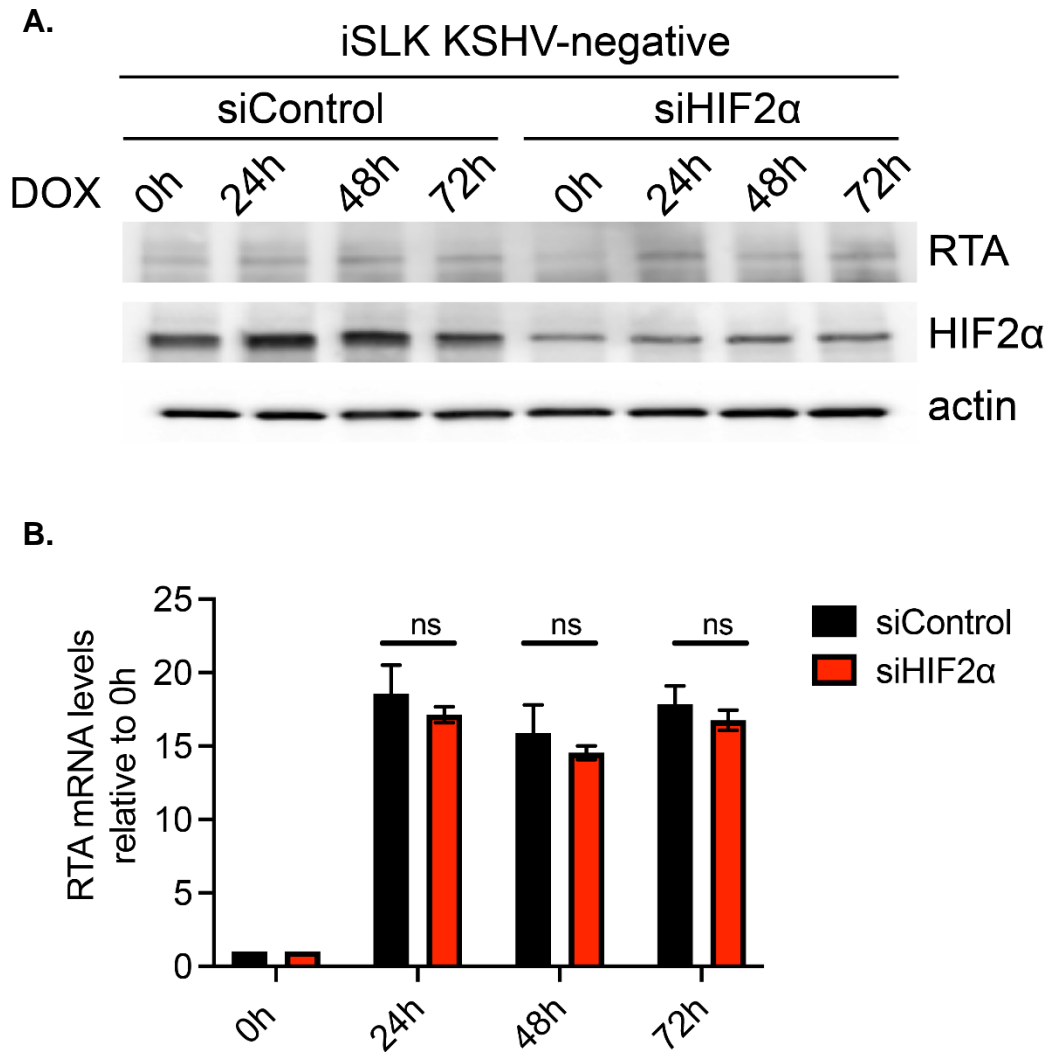


**Figure S3| HIF2 $\alpha$  silencing does not affect DOX induction of exogenous RTA in iSLK cells, related to Figure 1. A)** Inducible levels of RTA protein in HIF2 $\alpha$  silenced iSLK cells lacking KSHV and only containing a DOX-inducible RTA plasmid. **B)** DOX-inducible RTA mRNA levels in cells from (A) relative to 0h, measured by qRT-PCR (n=3, mean $\pm$  SD, ns= not significant, 2-way ANOVA with Sidak's post-test).

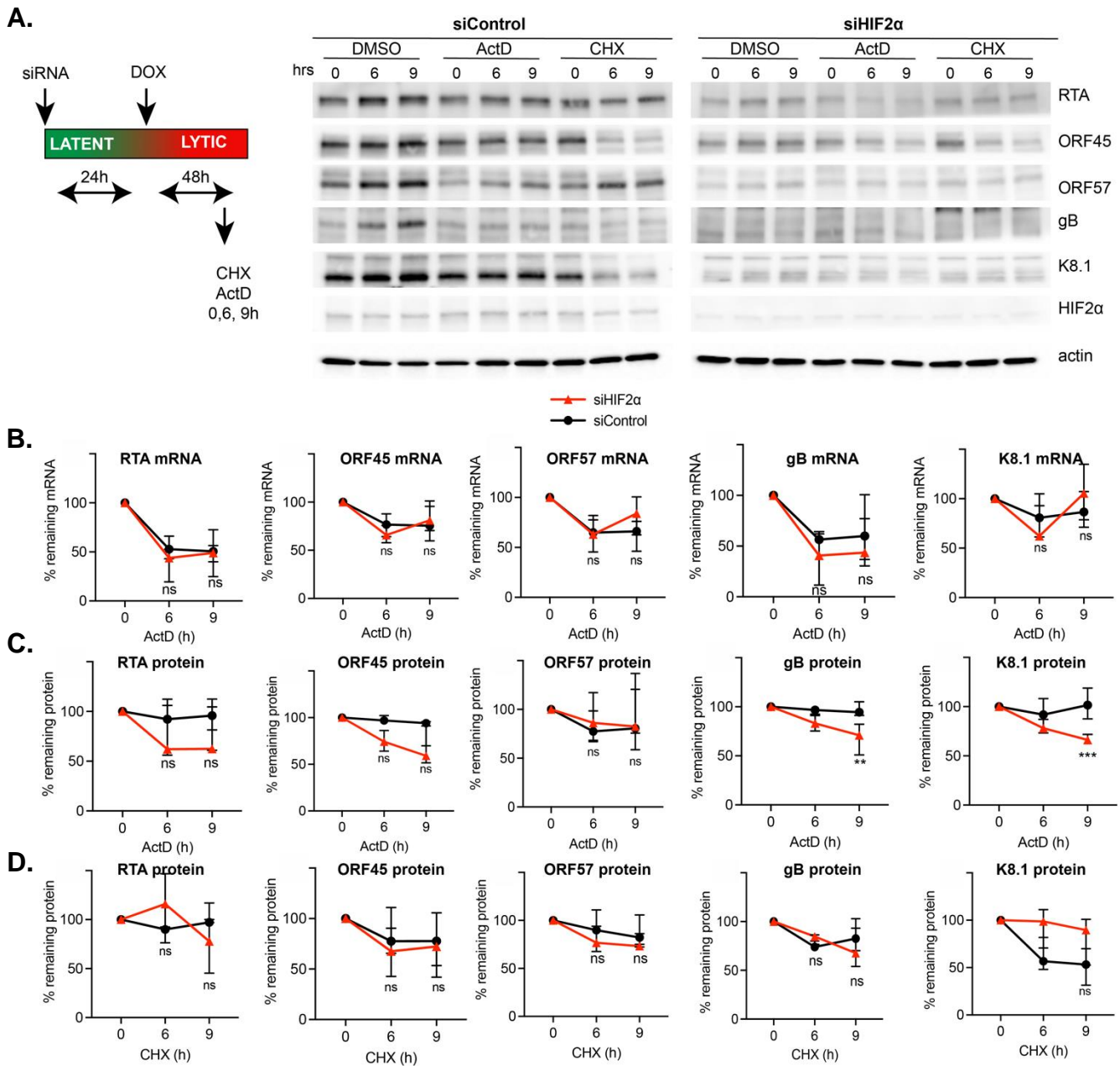


**Figure S4| HIF2 $\alpha$  plays a post-transcriptional role during KSHV replication, related to Figure 1. A)** Representatives immunoblots of actinomycin D (ActD) and cycloheximide (CHX) treated lytic iSLK.KSHV219 for 0, 6 and 9 h. iSLK.KSHV219 cells were silenced as in Figure 1 and 48 h post-reativation were treated with ActD and CHX. **B)** Remaining viral mRNA level after 9 h timecourse of ActD treatment in cells from (A). Viral mRNAs were measured by qRT-PCR (n=3, median with range, ns= not significant, 2-way ANOVA with Sidak's post-test). **C)** Expression of viral proteins in ActD treated iSLK.KSHV219 from (A) (n=3, median with range, \* p< 0.01, 2-way ANOVA with Sidak's post-test). **D)** Viral protein level in cells from (A) after CHX treatment (n=3, median with range, ns= not significant, 2-way ANOVA with Sidak's post-test).



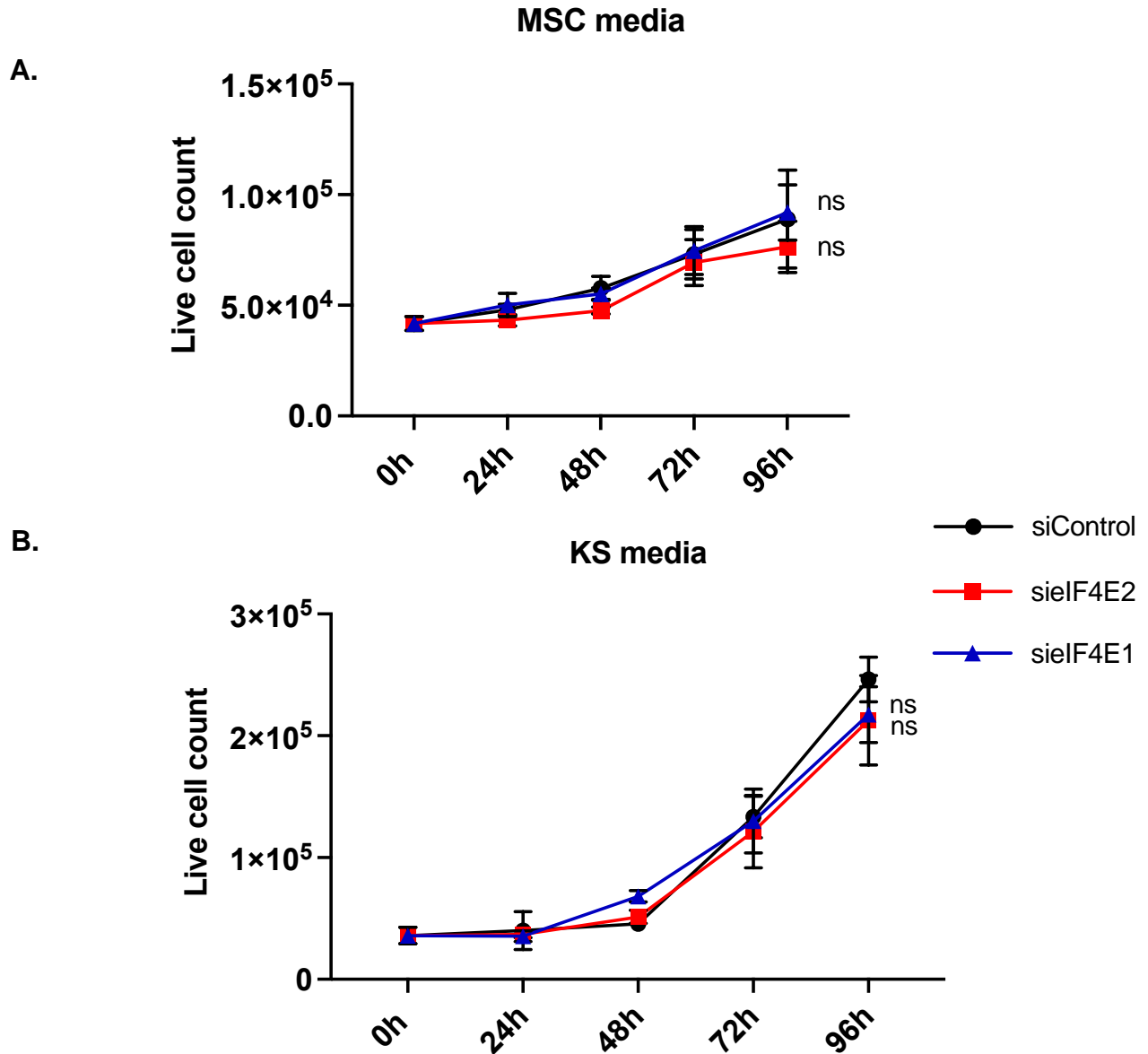


**Figure S5| Silencing of cap-binding proteins has no effect in the proliferation of KSHV-negative hMSCs, related to Figure 6 and Figure 7. A)** 96 h timecourse of live cell count of silenced KSHV-negative hMSC cultured in MSC media ( $n=3$ , mean $\pm$  SD, ns= not significant, 2-way ANOVA with Tukey's multiple comparisons post-test). **B)** Live KSHV-negative hMSC count silenced with siControl, siF4E2 and siF4E1 and cultured in KS media for 96 h ( $n=3$ , mean $\pm$  SD, ns= not significant, 2-way ANOVA with Tukey's multiple comparisons post-test).

## SUPPLEMENTAL TABLES

**Table S1: Primer sequences used to determine mRNA transcript levels for specific genes, related to STAR METHODS.**

Gene name	Forward Primer (5' to 3')	Reverse Primer (5' to 3')
Human $\beta$ -actin	CTCTTCCAGCCTTCCTTCCTG	CAGCACTGTGTTGGCGTACAG
KSHV RTA	CAAGGTGTGCCGTGTAGAGA	TCCCAAAGAGGTACCAGGTG
KSHV ORF45	CATGGGATGGGTAGTCAGG	GGGTCGCTGTATGGTGAAC
KSHV ORF57	GACCACGCGACCGCCTACAATACG	ATGGTGGGGCGGGAATGAAGACA
KSHV K8.1	CACCACAGAACTGACCGATG	TGGCACACGGTTACTAGCAC
KSHV gB	CTGGGGACTGTCATCCTGTT	ATGCTTCCTCACCAGGTTTG
KSHV ORF34	ACCCCTTCCGTTGCTATG	ACAGTCGGCCCGACAAAA
Human HIF2 $\alpha$	GCGGGACTTCTTCATGAGGATG	GAGGAGGGCAGTTGTTGTAGAC
Human eIF4E2	TCCCGTTGCTGGGAGAATCTCA	GTTGCTTGGTCACTGGCAGTCT
Human RPL3	CCGCACTGAGATCAACAAGA	CAGCCTTTCAGCATGACAAA
Human ATP5H	GCTGCTTTACCTGAGAATCCACC	TATCCTCTGGCACGGGAACCTT
Human RBM3	GACCACTTCAGCAGTTTCGGAC	TGGCTCTCATGGCAACTGAAGC
Human hnRNPC	GGAGATGTACGGGTCAGTAACA	CCCGAGCAATAGGAGGAGGA
Human RPL32	CGGCACCAGTCAGACCGATATG	GGGCAGCATGTGCTTTGTTTTTT
Human RHOA	CCATCATCCTGGTTGGGAAT	CCATGTACCCAAAAGCGC